

Falcon-X: A Time Series Foundation Model for Heterogeneous Multivariate Modeling

Yiding Liu*, Yifan Hu*, Hongjie Xia*, Peiyuan Liu*, Hongzhou Chen, Xilin Dai, Zewei Dong[†], Jiangming Yang

*Equal Contribution, [†]Corresponding Author, ✉ {yiding.lyd, zewei.dong}@ant-intl.com

Time series foundation models (TSFMs) are transforming the forecasting paradigm through large-scale cross-domain pretraining. However, most existing TSFMs remain univariate, and recent efforts to enable cross-variate modeling still operate directly within the raw variate space. This design introduces fundamental limitations in semantic alignment and relational expressivity. Specifically, raw-space group mixing lacks a dedicated mechanism to align heterogeneous physical quantities, while standard non-negative attention fails to capture the complex synergistic and antagonistic interactions ubiquitous in real-world systems. To address these challenges, we propose **Falcon-X**, decouples variates from the raw space and maps them into a unified latent prototype space. **Falcon-X** employs a Unified Prototype Diff-Attention mechanism that explicitly evaluates both positive and negative semantic affinities to explicitly align heterogeneous variates. Cross-variate interactions are then efficiently performed within this shared space via Latent Entity Attention, naturally facilitating zero-shot structural transfer. Finally, a Variate Reassembly Router robustly reconstructs variate-specific trajectories via a request-and-dispatch mechanism. Extensive evaluations on the GIFT-Eval and fev-bench benchmarks demonstrate that **Falcon-X** achieves state-of-the-art forecasting performance, offering a principled and scalable paradigm for complex multivariate environments. **Falcon-X** is publicly released to support future research.

Date: May 27, 2026

Code: <https://github.com/ant-intl/Falcon-TST>

Model: Coming soon.



1 Introduction

Time series forecasting is a fundamental task for understanding dynamic systems and supporting future-oriented decision making. Conventional deep forecasting models are typically trained at the dataset level (Kong et al., 2025), making them difficult to reuse across domains, sampling frequencies, and variate structures that vary in the real world. Time series foundation models (TSFM) are reshaping this paradigm by pretraining on large-scale cross-domain data and transferring directly to new forecasting tasks (Kottapalli et al., 2025), thereby substantially reducing the cost of repeated training and tuning. However, most existing models still take univariate series as the basic modeling unit, extrapolating the future solely from each series’ own history. This formulation disconnects the co-evolving relationships that are ubiquitous in real systems, limiting the ability of TSFMs to capture complex multivariate dynamics.

To enable cross-variate modeling, recent TSFMs explore how foundation models can accommodate varying numbers of variates. As shown in Table 1, Moirai-1.0 (Woo et al., 2024) flattens multivariate series into a single sequence, enabling joint attention across time and variates. While straightfor-

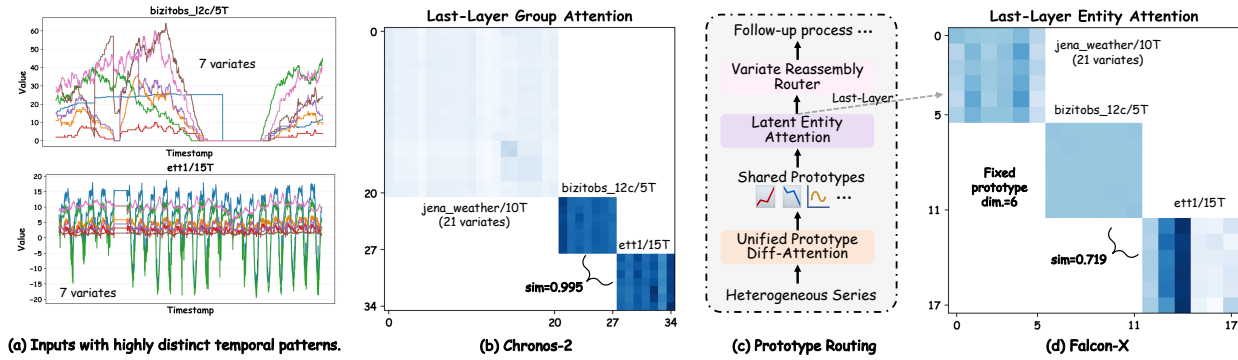


Figure 1 Comparison of multivariate modeling paradigms. (a) Heterogeneous inputs with highly distinct temporal patterns. (b) Group attention produces almost identical attention maps for completely dissimilar inputs, exposing the severe semantic collapse and over-smoothing in the raw variate space. (c-d) In contrast, **Falcon-X** projects variates into a latent prototype space, yielding highly discriminative attention maps that accurately capture the underlying dynamics.

ward, this design scales poorly with the number of variates, as attention cost increases rapidly in high-dimensional settings. A more effective alternative is group attention (Cohen et al., 2025; Ansari et al., 2025), which organizes variates into dataset-, entity-, or task-level groups and confines attention to variates within the same group. This avoids indiscriminate mixing across unrelated samples while allowing a shared backbone to process multivariate inputs with varying dimensionalities. By replacing global all-to-all interaction with structured within-group communication, group attention marks an important step toward scalable multivariate TSFMs.

However, group attention still exhibits fundamental limitations in *semantic alignment* and *relational expressivity*. ❶ It operates directly in the raw variate space, controlling which variates can interact but not how their heterogeneous semantics are aligned. In high-dimensional systems, only a small subset of variates typically exhibits strong dependencies, while many others are weakly related or noisy. As shown in Figure 1, Dense attention over raw variates can therefore dilute meaningful signals and promote dataset-specific correlations as if they were transferable patterns. Moreover, different datasets share the same Transformer backbone, yet their variates often correspond to entirely different physical quantities and dynamics. Without an dedicated alignment space, the model must absorb such heterogeneity implicitly in its parameters, making cross-domain transfer a by-product of parameter sharing rather than an principled process of organizing reusable temporal structures. ❷ Existing attention mechanisms have limited relational expressivity. In real-world systems, cross-variate dependencies often involve both synergistic and antagonistic interactions. However, current attention formulations primarily capture aggregative effects, lacking the ability to represent opposing dynamics and more complex interaction patterns.

In this paper, we address these limitations by decoupling physical variates from the latent space used for cross-variate interaction. Instead of mixing raw variates, we map them into a shared fixed-dimensional latent prototype space, where interactions are mediated by pairs of learnable prototypes that explicitly capture both positive and negative semantic affinities. These prototypes absorb recurring temporal structures across datasets and filter out variate-specific noise, enabling the model to learn reusable cross-domain patterns in an unified aligned space. This alignment establishes a common semantic coordinate system for heterogeneous variates, making cross-domain interactions more structured, transferable, and scalable. It also replaces dense variate-level attention with lightweight variate-to-prototype interaction, substantially improving efficiency while preserving cross-variate modeling capacity.

Technically, we propose **Falcon-X**, a novel encoder-only TSFM with 591 million parameters materializing this latent prototype paradigm for heterogeneous multivariate forecasting. At its core, the Unified Prototype Diff-Attention decouples heterogeneous variates into a fixed semantic space, utilizing a differential mechanism to explicitly capture both synergistic and antagonistic variate relationships. Once aligned, the Latent Entity Attention performs global cross-variate interactions entirely within this unified space, naturally facilitating seamless cross-domain transfer without coupling to raw variate dimensions. To project back to the original physical space, a dynamic Variate Reassembly Router robustly reconstructs variate-specific trajectories via a *request-and-dispatch* mechanism and gated residual connections. Furthermore, **Falcon-X** integrates essential instance-wise normalization, patching, and a probabilistic forecasting head to ensure end-to-end stability. Extensive experiments on the GIFT-Eval (Aksu et al., 2024) and fev-bench (Shchur et al., 2025) validate that **Falcon-X** advances the state-of-the-art in scalable and zero-shot multivariate forecasting.

In a nutshell, our main contribution can be summarized as:

- ***A Novel Heterogeneous Modeling Paradigm.*** We present a paradigm shift for multivariate time series foundation models, moving from raw-space mixing to a unified latent prototype space. This approach elegantly resolves semantic discrepancies across different datasets, creating a universal coordinate system that naturally facilitates zero-shot knowledge transfer.
- ***Architectural Innovation.*** We propose **Falcon-X**, a tailored encoder-only foundation model. It features a Differential Prototype Attention which comprehensively captures both synergistic and antagonistic system dynamics, together with a gated Variate Reassembly Router that adaptively regulates global context fusion for cross-dataset robustness.
- ***Empirical Excellence.*** Through extensive evaluations on comprehensive widely used benchmarks (GIFT-Eval and fev-bench), **Falcon-X** consistently achieves state-of-the-art forecasting performance. The results validate its superior structural adaptability and broad generalization capabilities in complex multivariate environments.

2 Related Works

In recent years, the emergence of pre-training techniques has shifted the paradigm of time series forecasting from domain-specific models to the era of foundation models. Early explorations in this domain, such as Time-LLM (Jin et al., 2023), primarily focused on tuning third-party large language models to adapt time series tasks. Subsequently, with the accumulation of massive time series data, the trend has transitioned toward learning from scratch, where models are pre-trained directly on large-scale time series data to capture inherent temporal dynamics. Chronos (Ansari et al., 2024) frames time series forecasting as a language modeling task by tokenizing real-valued observations into a discrete vocabulary. MOMENT (Goswami et al., 2024) introduces a family of foundation models using a masked prediction task, which allows for generalization across time series tasks through fine-tuning. Inspired by the success of large language models, the generative paradigm built upon decoder-only architectures has become a prominent choice for many mainstream works. These methods typically partition time series into non-overlapping patches, treating each patch as a single token (Nie et al., 2023), and leverage decoder-only structures to generate one patch at each step (Liu et al., 2024; Das et al., 2024; Liu et al., 2025a,b; Auer et al., 2025). Despite achieving competitive zero-shot performance, these models primarily rely on the channel independence strategy, which limits them to univariate forecasting and ignores the rich context of multivariate dependencies found in real-world time series data.

Table 1 Comparison of capabilities of TSFMs.

TSFMs	Falcon-X	Moirai 2.0	TimesFM-2.5	Chronos-2	Timer-S1	Toto	Sundial	Moirai 1.0	TabPFN-TS
	(Ours)	(2025a)	(2024)	(2025)	(2026)	(2025)	(2025b)	(2024)	(2025)
Univariate	✓	✓	✓	✓	✓	✓	✓	✓	✓
Multivariate	✓	✗	✗	✓	✗	✓	✗	✓	✗
Cross Learning ¹	✓	✗	✗	✓	✗	✗	✗	✗	✗
Signed Dependence ²	✓	✗	✗	✗	✗	✗	✗	✗	✗
Heterogeneous Unification ³	Prototype Routing	✗	✗	Group Mixing	✗	Fixed	✗	Concat.	✗

¹Transferring of universal cross-variate interactive patterns across distinct datasets.

²Computing both positive and negative affinities to capture synergistic and antagonistic dynamics.

³Projecting physical variates with varying dimensionalities into a dimension-agnostic latent space.

Despite these advances, a key challenge of multivariate forecasting remains the unified modeling of heterogeneous time series. Moirai 1.0 (Woo et al., 2024) flattens variates into a single sequence to capture joint interactions. Toto (Cohen et al., 2025) introduces proportional factorized space-time attention to efficiently model cross-variate dependency. Furthermore, Chronos-2 (Ansari et al., 2025) further adopts group attention, facilitating in-context learning by sharing information across related series within flexible groups. However, these approaches still operate directly within the raw variate space, fundamentally limiting their semantic alignment and relational expressivity. Specifically, they primarily capture aggregative effects and struggle to represent the antagonistic dynamics ubiquitous in real-world physical systems. To bridge this gap, our **Falcon-X** introduces a differential mechanism within an explicitly aligned latent prototype space, enabling the foundation model to systematically capture complex dual dynamics and facilitate robust cross-domain transfer.

3 Falcon-X

In this section, we present the architecture of **Falcon-X**. As shown in Figure 2, **Falcon-X** consists of four parts: pre-process of Normalization and Tokenization, Time Attention, Variate Attention and Forecasting Head. To maintain a concise exposition of the mathematical formulations, we present extended discussions of our *underlying design philosophies* in Appendix A.

3.1 Problem Formulation

Let $\mathcal{E} = \{\mathbf{e}_i \in \mathbb{R}^{m_i \times L}\}_{i=1}^N$ be a collection of N entities, where each entity \mathbf{e}_i represents a multivariate time series with a specific variate dimensionality m_i and a historical look-back window L . A key challenge in TSFM is the heterogeneity of these dimensions, with m_i varying significantly across diverse entities and datasets. We define the total aggregated dimensionality M across all entities as $\sum_{i=1}^N m_i$. The objective of **Falcon-X** is to learn a dimension-agnostic mapping \mathcal{F}_θ , parameterized by θ , that transforms the heterogeneous input space into the target predictive space:

$$\hat{\mathbf{Y}} = \mathcal{F}_\theta(\mathbf{X}), \quad \text{where } \mathbf{X} \in \mathbb{R}^{M \times L}, \hat{\mathbf{Y}} \in \mathbb{R}^{M \times T}. \quad (1)$$

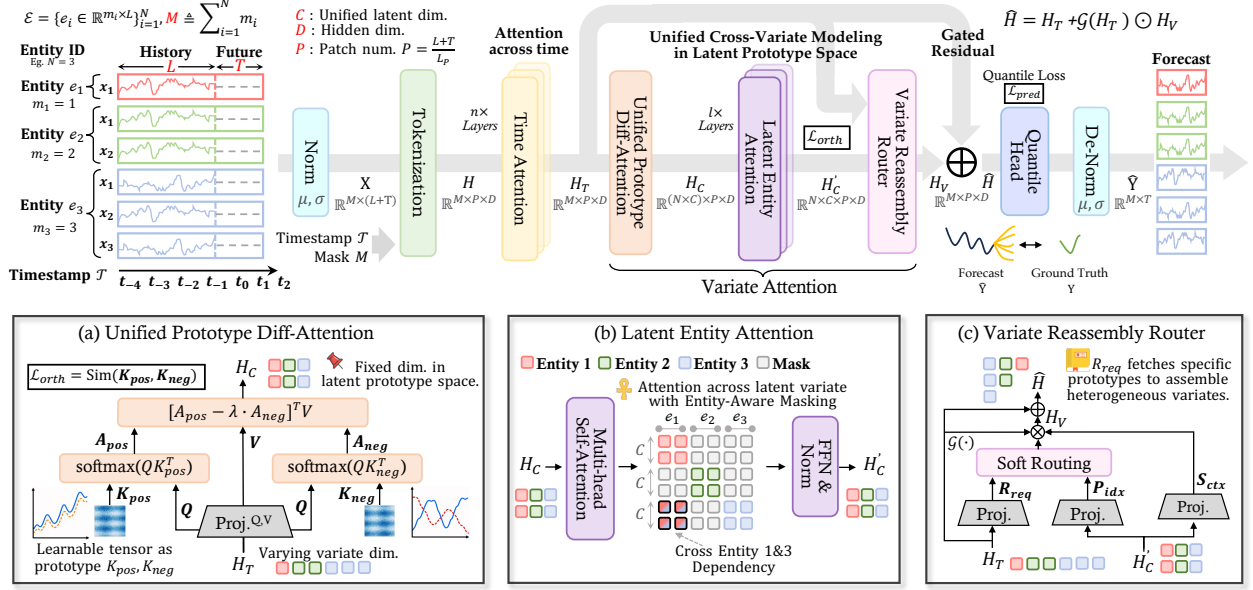


Figure 2 The overall architecture of **Falcon-X**. The raw inputs are normalized, tokenized, and processed by Time Attention to extract independent temporal features. The Unified Prototype Diff-Attention (UPDA) then projects these features into a shared prototype space, enabling Latent Entity Attention (LEA) to capture global cross-variate dependencies explicitly. The Variate Reassembly Router (VRR) then dynamically reconstructs variate-specific representations. These are fused with the temporal context and fed into a quantile head to generate the final probabilistic forecasts.

3.2 Normalization and Tokenization

Normalization. We formulate the forecasting task as a unified masked reconstruction paradigm. Given the raw input $X \in \mathbb{R}^{M \times (L+T)}$ spanning the historical window L and future horizon T , we first replace the target future steps with placeholder tokens. To ensure scale-invariance across diverse domains, we apply an arcsine transformation:

$$\hat{X} = \arcsin\left(\frac{X - \mu}{\sigma}\right). \quad (2)$$

Crucially, instead of zero-filling or truncating sequences at missing positions (Xiaoming et al., 2025), the instance-wise mean μ and standard deviation σ are computed exclusively from observed values, preserving missing entries for explicit downstream modeling.

Tokenization. To obtain robust representations, we augment \hat{X} by concatenating it with a relative timestamps \mathcal{T} and a binary observation mask \mathcal{M} . To generalize across heterogeneous sampling frequencies, \mathcal{T} injects a normalized sequential ordering anchored at 0 for the first forecasting step:

$$\mathcal{T} = \left\{-\frac{L}{L+T}, \dots, 0, \dots, \frac{T-1}{L+T}\right\}. \quad (3)$$

Meanwhile, the explicit inclusion of \mathcal{M} enables the model to dynamically distinguish genuine observations from missing entries or masked future targets. Subsequently, the augmented sequence is partitioned into $P = \frac{L+T}{L_p}$ non-overlapping patches of length L_p and projected into the hidden dimension D via a residual patch embedding mechanism:

$$\mathbf{H} = \text{ResPatchEmbed}(\text{Concat}(\hat{X}, \mathcal{T}, \mathcal{M})) \in \mathbb{R}^{M \times P \times D}. \quad (4)$$

Unlike standard linear projections, the residual patch embedding is designed to seamlessly integrate linear properties with the complex non-linear semantics extracted from the augmented inputs.

3.3 Time Attention

To capture the intrinsic evolutionary patterns of each individual variate, **Falcon-X** utilizes an encoder-only Transformer architecture (see Appendix A.2). Specifically, the Time Attention module consists of n identical encoder layers, each applied independently along the time dimension D for all M variates. Let $\mathbf{H}^{(0)} = \mathbf{H}$ be the input from the Tokenization layer. For each layer $i \in \{1, \dots, n\}$, the hidden state $\mathbf{H}^{(i)}$ is computed as follows:

$$\mathbf{H}^{(i)} = \text{LayerNorm} \left(\mathbf{H}^{(i-1)} + \text{MHA} \left(\mathbf{H}^{(i-1)} \right) \right), \quad (5)$$

where MHA denotes the multi-head attention mechanism (Vaswani et al., 2017). We apply LayerNorm (Ba et al., 2016) to every layer to stabilize the internal activations and facilitate the training of deep foundation architectures. After n successive transformations, the final output is denoted as $\mathbf{H}^{(n)} = \mathbf{H}_T \in \mathbb{R}^{M \times P \times D}$, encapsulating the comprehensive temporal dynamics of each variate.

3.4 Variate Attention

A core requirement of time-series foundation models is *the ability to transcend rigid, dataset-specific dimensional constraints and learn a unified representation of dependencies across multi-variat series*. However, treating different physical variates homogeneously or simply concatenating them leads to severe semantic misalignment. To overcome this, **Falcon-X** introduces a unified latent space paradigm. As shown in Figure 2(a–c), these modules progressively aligns the heterogeneous patch embeddings \mathbf{H}_T into a shared prototype space, models both intra- and cross-dataset dependencies, and dynamically reassembles the global context back to the original variate dimensions.

3.4.1 Unified Prototype Diff-Attention

To overcome the semantic misalignment inherent in raw-space interactions (detailed discussion in Appendix A.3.1), **Falcon-X** projects the heterogeneous temporal embeddings H_T into a fixed- C -dimensional latent prototype space. We employ a Differential Attention mechanism to explicitly capture both positive and negative semantic affinities.

Concretely, we define two globally shared learnable parameter matrices, $\mathbf{K}_{\text{pos}}, \mathbf{K}_{\text{neg}} \in \mathbb{R}^{C \times D}$, representing the synergistic and antagonistic temporal prototypes, respectively. For each entity e_i , given its temporal embeddings $\mathbf{h}_T^i \in \mathbb{R}^{m_i \times P \times D}$, we generate the query \mathbf{Q}^i and value \mathbf{V}^i via linear projections. The dual-dependency attention maps, quantifying the affinity between the m_i heterogeneous variates of the i -th entity and the C unified prototypes, are computed as:

$$\mathbf{A}_{\text{pos}}^i = \text{softmax} \left(\frac{\mathbf{Q}^i \mathbf{K}_{\text{pos}}^\top}{\sqrt{D}} \right), \quad \mathbf{A}_{\text{neg}}^i = \text{softmax} \left(\frac{\mathbf{Q}^i \mathbf{K}_{\text{neg}}^\top}{\sqrt{D}} \right), \quad (6)$$

where $\mathbf{A}_{\text{pos}}^i, \mathbf{A}_{\text{neg}}^i \in \mathbb{R}^{m_i \times P \times C}$. The unified representation $\mathbf{h}_C^i \in \mathbb{R}^{C \times P \times D}$ for entity e_i is then derived by aggregating the value features based on the differential attention score:

$$\mathbf{h}_C^i = \left[\mathbf{A}_{\text{pos}}^i - \lambda \cdot \mathbf{A}_{\text{neg}}^i \right]^\top \mathbf{V}^i, \quad (7)$$

where λ is a learnable scaling factor and $\mathbf{V}^i = \text{Linear}(\mathbf{h}_T^i)$. Notably, while this projection is logically defined at the individual entity level, we implement it concurrently across all N entities to maximize computational efficiency. By employing an entity-aware masking strategy, we completely bypass inefficient explicit loops, seamlessly and parallelly transforming the heterogeneous inputs into

a perfectly unified latent space $\mathbf{H}_C \in \mathbb{R}^{N \times C \times P \times D}$. To ensure semantic distinctiveness, we apply an orthogonality loss $\mathcal{L}_{\text{orth}} = \text{Sim}(\mathbf{K}_{\text{pos}}, \mathbf{K}_{\text{neg}})$ to constrain the relationship between positive and negative prototypes, where $\text{Sim}(\cdot, \cdot)$ denotes the normalized cosine similarity.

3.4.2 Latent Entity Attention

With all representations $\mathbf{H}_C \in \mathbb{R}^{(N \times C) \times P \times D}$ aligned into a shared, dimension-agnostic semantic space, Latent Entity Attention naturally facilitates cross-learning, leveraging shared structural patterns across entirely different domains (see Appendix A.3.2). To be specific, we treat the combined entity and prototype dimensions as the spatial sequence for interaction, and then apply l layers of the standard MHA mechanism to capture the global cross-variate dependencies:

$$\mathbf{H}'_C = \text{LayerNorm}(\mathbf{H}_C + \text{MHA}(\mathbf{H}_C)), \quad (8)$$

where $\mathbf{H}'_C \in \mathbb{R}^{N \times C \times P \times D}$ denotes the refined global context matrix. Similar to the Time Attention, this straightforward yet highly effective operation utilizes residual connections and layer normalization to ensure stable representations. By allowing all aligned entities to interact fully within this latent space, \mathbf{H}'_C successfully captures the holistic dynamics necessary for accurate forecasting.

3.4.3 Variate Reassembly Router

To accurately reconstruct variate-specific trajectories, **Falcon-X** orchestrates a targeted retrieval from the unified prototype space back to individual physical dimensions (m_i) via a *request-and-dispatch* mechanism (see Appendix A.3.3). Formally, for each entity \mathbf{e}_i , we generate the routing components through independent linear projections based on their respective source tensors:

$$\mathbf{R}_{\text{req}}^i = \text{Linear}(\mathbf{h}_T^i), \quad \mathbf{P}_{\text{idx}}^i = \text{Linear}(\mathbf{h}_C^i), \quad \mathbf{S}_{\text{ctx}}^i = \text{Linear}(\mathbf{h}_C^i). \quad (9)$$

Here, the Routing Request ($\mathbf{R}_{\text{req}}^i$) acts as an *entity identity tag* conveying the unique temporal trajectory of the original variate. It is matched against the Prototype Index ($\mathbf{P}_{\text{idx}}^i$), an addressable map of the global prototype library, to selectively retrieve refined semantic payloads from the Source Context ($\mathbf{S}_{\text{ctx}}^i$). Rather than performing dense token-level interaction, the reconstruction is then executed via a scaled dot-product soft-routing operation, where each variate dynamically allocates its representation across a compact set of latent prototypes:

$$\mathbf{h}_V^i = \text{Route}(\mathbf{R}_{\text{req}}^i, \mathbf{P}_{\text{idx}}^i) \mathbf{S}_{\text{ctx}}^i = \text{softmax} \left(\frac{\mathbf{R}_{\text{req}}^i (\mathbf{P}_{\text{idx}}^i)^\top}{\sqrt{D}} \right) \mathbf{S}_{\text{ctx}}^i. \quad (10)$$

This retrieval paradigm successfully reconstructs variate-specific $\mathbf{h}_V^i \in \mathbb{R}^{m_i \times P \times D}$ with high fidelity, smoothly restoring the physical dimensionality to yield $\mathbf{H}_V \in \mathbb{R}^{M \times P \times D}$. Similar to the initial prototype projection, we apply an entity-aware masking strategy during routing, enabling concurrent soft routing across all N entities without explicit loops.

Finally, to maintain robust cross-dataset performance regardless of varying dependency strengths, we introduce an explicit gated residual connection to dynamically fuse the temporal embeddings \mathbf{H}_T with the cross-variate representations \mathbf{H}_V . The final output $\hat{\mathbf{H}} \in \mathbb{R}^{M \times P \times D}$ is computed as:

$$\hat{\mathbf{H}} = \mathbf{H}_T + \mathcal{G}(\mathbf{H}_T) \odot \mathbf{H}_V, \quad (11)$$

where $\mathcal{G}(\cdot)$ is a gating mechanism with a linear projection followed by a sigmoid activation, and \odot is element-wise multiplication. Thus, **Falcon-X** effectively prevents semantic interference in weakly correlated systems while making full use of cross-variate dependencies in strongly correlated ones.

3.5 Forecasting Head

Following Chronos-2 (Ansari et al., 2025) and Timer-S1 (Liu et al., 2026), **Falcon-X** adopts a probabilistic forecasting paradigm, predicting future distributions instead of deterministic point estimates. Given the reconstructed representation $\hat{\mathbf{H}}$, we extract the embeddings corresponding to the masked future horizon and apply a linear projection to generate forecasts across a predefined set of quantiles \mathcal{Q} . The model is end-to-end optimized using the standard Quantile Loss:

$$\mathcal{L}_{\text{pred}} = \frac{1}{|\mathcal{Q}| \cdot M \cdot T} \sum_{q \in \mathcal{Q}} \sum_{i=1}^M \sum_{t=1}^T \max \left(q(\mathbf{Y}_{i,t} - \hat{\mathbf{Y}}_{i,t}^{(q)}), (q-1)(\mathbf{Y}_{i,t} - \hat{\mathbf{Y}}_{i,t}^{(q)}) \right), \quad (12)$$

where $\mathbf{Y}_{i,t}$ represents the ground truth and $\hat{\mathbf{Y}}_{i,t}^{(q)}$ denotes the model’s prediction at the q -th quantile. The overall training objective combines this with the prototype orthogonality loss: $\mathcal{L} = \mathcal{L}_{\text{pred}} + \alpha \mathcal{L}_{\text{orth}}$, where α is a hyper-parameter balancing the forecasting and orthogonality objectives.

During inference, the predictions are mapped back to their original physical scale $\tilde{\mathbf{Y}}^{(q)}$ via a straightforward de-normalization process, applying the sine transformation followed by De-Norm using the preserved instance-wise statistics.

$$\tilde{\mathbf{Y}}^{(q)} = \sigma \cdot \sin(\hat{\mathbf{Y}}^{(q)}) + \mu. \quad (13)$$

4 Training Details

4.1 Pre-Training Corpus

Our pre-training corpus combines large-scale real-world and synthetic time series data spanning several domains. In addition to public datasets from GIFT-EVAL (Aksu et al., 2024), CHRONOS (Ansari et al., 2024) and QUITOBENCH (Xue et al., 2026), it includes synthetic univariate and multivariate series designed to increase diversity in temporal patterns and dependency structures. Specifically, synthetic univariate data are generated through data mixing and stochastic process sampling, while multivariate series are constructed by grouping related univariate signals and injecting explicit cross-variate dependencies, including both instantaneous and temporal interactions. The details can be found in Appendix B.1.

4.2 Training Infrastructure and Config

To enable scalable pretraining on massive, heterogeneous time-series corpora, we build **Falcon-X** upon Megatron-LM (Shoeybi et al., 2019) and design a custom sampling pipeline to balance data distribution across diverse domains. Furthermore, to address the heterogeneity in variate dimensionality, we implement a runtime multivariate sampling strategy that dynamically balances the number of consuming variates per batch, thereby improving GPU utilization and training stability. Further implementation details are provided in Appendix C.

Falcon-X features a hidden dimension of $D = 1024$, a patch length of $L_p = 16$, and utilizes $n = 16$ Time Attention layers alongside $l = 16$ Entity Attention layers (16 heads per layer). By accommodating up to 512 input tokens and 30 output tokens, it achieves a maximum context length of $L = 8192$ and a prediction length of $T = 480$ in a single inference pass. The model is pre-trained on a cluster of NVIDIA B200-180GB GPUs for one million iterations with a global batch size of 384 using bf16 precision, optimized by a joint quantile and orthogonality loss. We adopt the AdamW optimizer (Loshchilov and Hutter, 2019) with $\beta_1 = 0.9$, $\beta_2 = 0.95$, and a weight decay

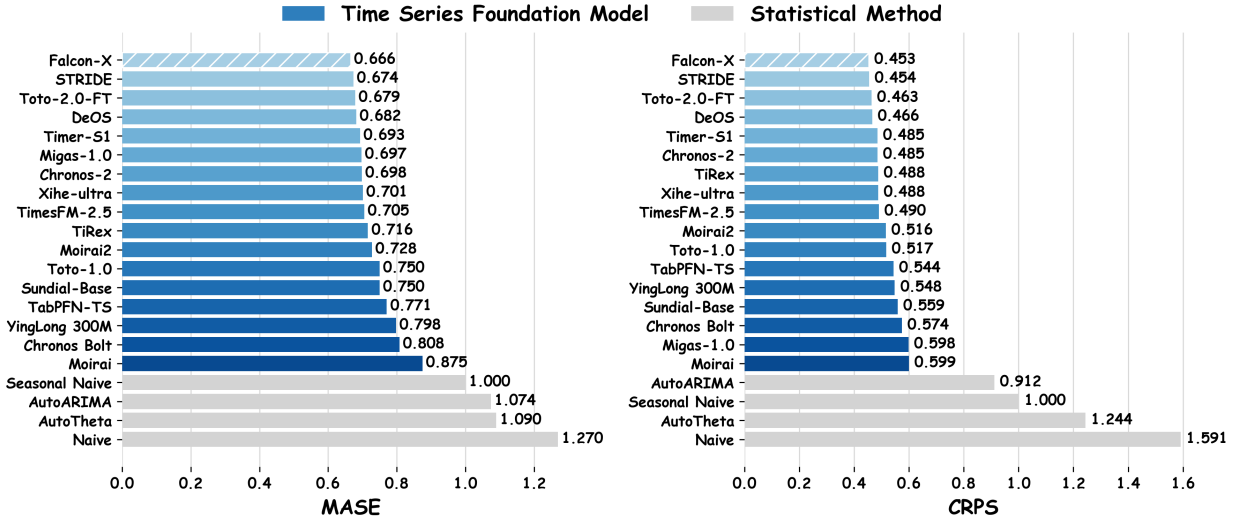


Figure 3 Performance of **Falcon-X** on the GIFT-Eval leaderboard. DeOS denotes DeOSAlphaTimeGPTPredictor-2025 and STRIDE denotes STRIDE+Chronos-2.

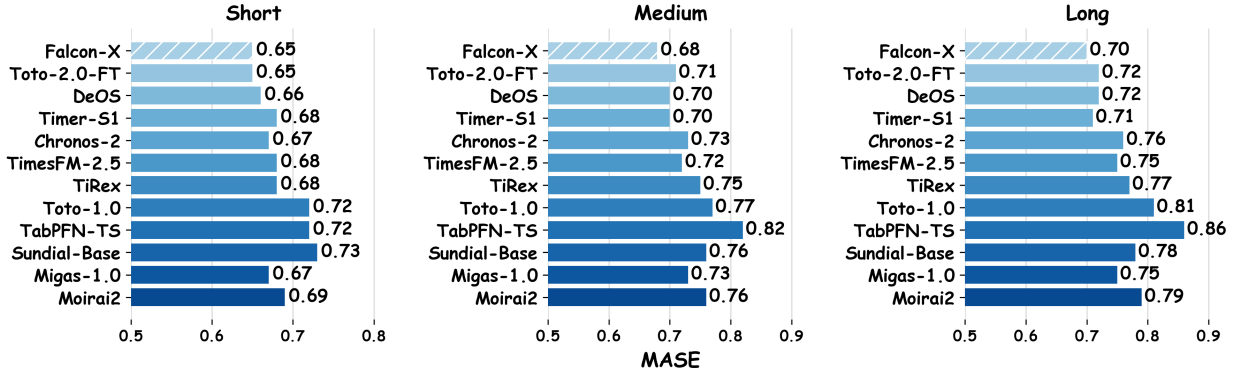


Figure 4 Performance (MASE) of **Falcon-X** on the GIFT-Eval leaderboard, grouped by the term length. **Falcon-X** exhibits remarkable stability across all horizons.

of 0.1. The learning rate warms up linearly to 6×10^{-5} over the first 0.1% of steps, followed by a cosine decay to 6×10^{-6} . As shown in Figure 6, the training process is highly stable, with the loss curve converging smoothly and robustly.

5 Experiments

5.1 Main Results

We evaluate Falcon-X on two comprehensive benchmarks, GIFT-Eval (Aksu et al., 2024) and fev-bench (Shchur et al., 2025), using MASE and CRPS to measure point forecasting accuracy and probabilistic calibration, respectively. As shown in Figure 3, Falcon-X achieves the best overall performance on GIFT-Eval, reaching 0.666 MASE and 0.453 CRPS. Compared with the strongest competing time-series foundation models, Falcon-X consistently delivers lower errors: it improves over STRIDE by 1.2% in MASE, over Toto-2.0-FT (Khwaja et al., 2026) by 1.9% in MASE and 2.2% in CRPS, and over Timer-S1 (Liu et al., 2026) by 3.9% in MASE and 6.6% in CRPS. It also surpasses representative multivariate TSFMs such as Chronos-2 (Ansari et al., 2025) and Toto-1.0 (Cohen et al., 2025), demonstrating that explicit latent prototype alignment is more effective than raw-space

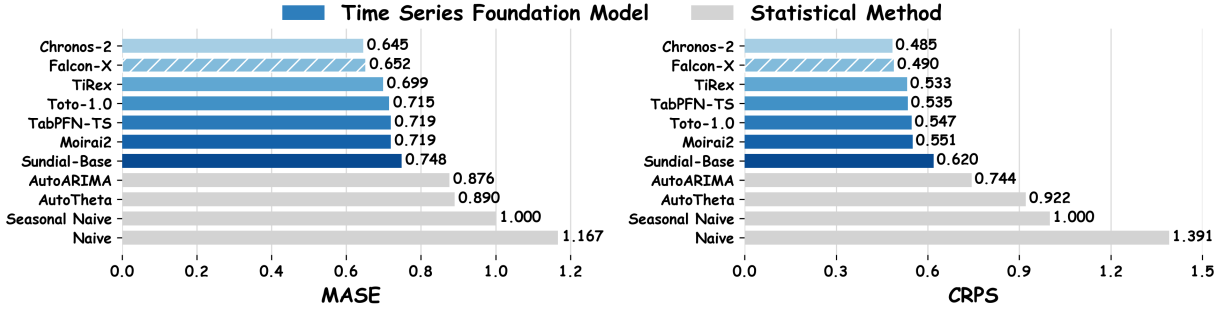


Figure 5 Performance of Falcon-X on the fev-bench leaderboard.

variate mixing for heterogeneous multivariate forecasting.

We further analyze the robustness of Falcon-X across different prediction horizons on GIFT-Eval. Figure 4 reports the MASE results grouped into short-, medium-, and long-term forecasting settings. Falcon-X obtains 0.65 MASE in the short-term setting, tying for the best result with Toto-2.0-FT (Khwaja et al., 2026). More importantly, its advantage becomes clearer as the forecasting horizon increases: Falcon-X achieves the best medium-term and long-term results, with 0.68 and 0.70 MASE, respectively. In contrast, Chronos-2 (Ansari et al., 2025) increases from 0.67 in the short-term setting to 0.76 in the long-term setting, while Toto-1.0 (Cohen et al., 2025) and TabPFN-TS (Hoo et al., 2025) degrade more substantially. These results indicate that Falcon-X not only performs well on immediate extrapolation, but also maintains stable predictive accuracy under extended horizons, suggesting that the latent prototype routing mechanism can capture durable cross-variate dynamics and mitigate horizon-wise error accumulation.

On fev-bench, Falcon-X also exhibits highly competitive generalization performance, as shown in Figure 5. Falcon-X ranks closely behind Chronos-2 (Ansari et al., 2025), achieving 0.652 MASE and 0.490 CRPS, compared with Chronos-2’s 0.645 MASE and 0.485 CRPS. The gap is only about 1.1% on MASE and 1.0% on CRPS, while Falcon-X relies strictly on endogenous target series rather than additional past-only or future-known covariates. Beyond Chronos-2 (Ansari et al., 2025), Falcon-X substantially outperforms other recent foundation models, including TiRex (Auer et al., 2025), Toto-1.0 (Cohen et al., 2025), Moirai 2.0 (Liu et al., 2025a), and so on. These results confirm that the proposed dual-dependency architecture provides strong relational expressivity and structural adaptability across diverse real-world forecasting tasks.

5.2 Ablation Studies

As shown in Figure 7(a), to isolate the contributions of the architecture and optimization pipeline, we conduct comprehensive ablation studies on both model components and training strategies.

Module Ablation. We first evaluate the structural designs of Falcon-X. (i) **Only K_{pos}** : Removing the negative prototype key (K_{neg}) causes the most severe performance drop, verifying that modeling negative affinities is essential for heterogeneous series interactions. (ii) **w/o gated residual**: Removing the gated residual connection degrades performance, showing its importance in context-aware filtering cross-variate information in various datasets. (iii) **w/o timestamp & mask**: Excluding the relative timestamp \mathcal{T} and mask \mathcal{M} reduces robustness to irregular sampling and missing values.

Strategy Ablation. We further analyze the impact of our data processing and training pipeline. (i) **w/o sampling shuffle**: Disabling variate shuffling significantly hurts performance, indicating

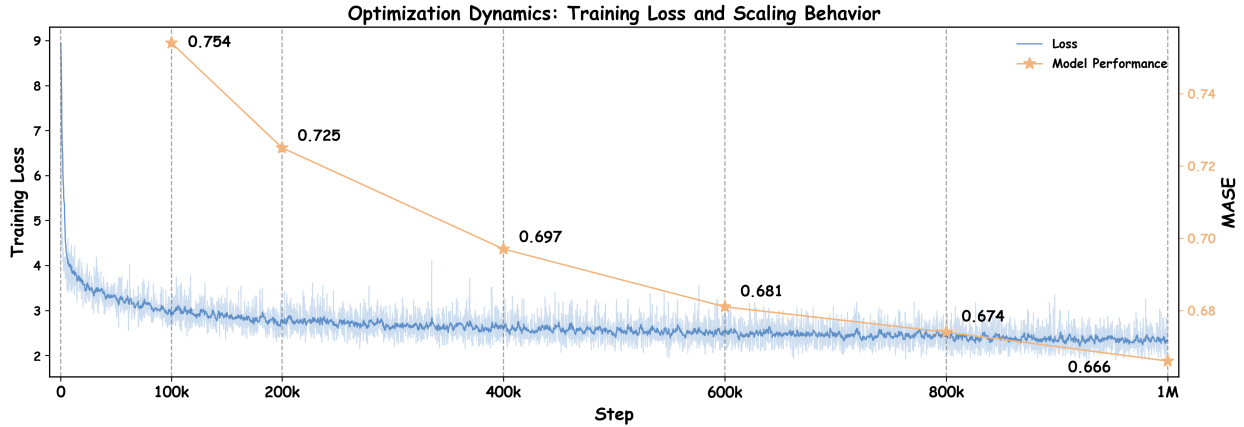


Figure 6 Stable training dynamics and performance scaling over one million iterations.

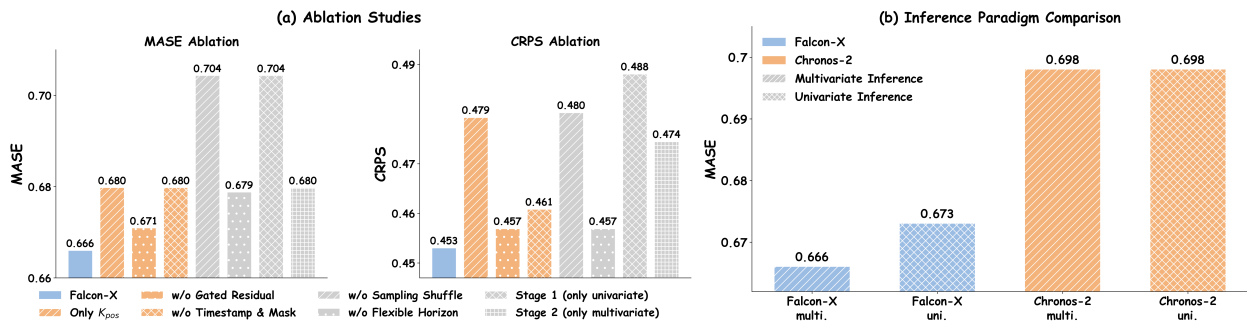


Figure 7 (a) Ablation studies validating the necessity of key architectural components and training strategies. (b) Inference paradigm comparison, highlighting our robust multivariate modeling against Chronos-2.

that random permutation is crucial for learning content-driven rather than index-dependent relationships. (ii) **w/o flexible horizon**: Replacing flexible horizon sampling with fixed-length prediction weakens generalization across unseen forecasting horizons. (iii) **Two-stage vs. Joint training**: We compare direct joint training with a two-stage curriculum consisting of: (Stage 1) univariate pre-training for temporal modeling initialization, and (Stage 2) multivariate fine-tuning with univariate replay. Joint training consistently performs better, indicating that **Falcon-X** can naturally unify temporal dynamics and cross-variate interactions within a single optimization process, without relying on carefully staged training curricula.

5.3 Inference Setting Analysis

We compare inference paradigms against Chronos-2 in Figure 7(b). On GIFT-Eval, Chronos-2 (Ansari et al., 2025) exhibits nearly identical performance regardless of whether its group attention is enabled, indicating that raw-space variate mixing contributes little effective relational information. This reveals a severe semantic collapse, where cross-variate interaction degenerates into univariate-like behavior. In contrast, enabling multivariate inference in **Falcon-X** consistently improves accuracy on multivariate tasks over its univariate inference mode, demonstrating that **Falcon-X** can effectively capture transferable cross-variate dependencies. Crucially, this cross-variate enhancement fully preserves the accuracy on univariate forecasting, proving that our latent routing successfully extracts global synergistic context without corrupting individual temporal signals.

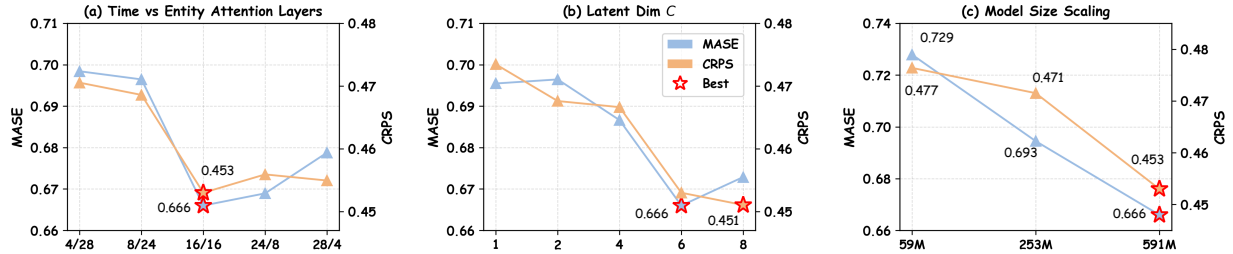


Figure 8 Sensitivity and scaling analysis. (a) Performance impact of layer allocation between Time Attention n and Entity Attention l . (b) Sensitivity to the latent prototype dimension C . (c) Consistent performance scaling across increasing model parameter sizes (from 59M to 591M).

5.4 Influence of Key Parameter

We analyze the sensitivity of **Falcon-X** to two key architectural parameters.

Depth Distribution (n vs. l). We investigate the layer allocation between Time Attention (n) and Latent Entity Attention (l) under a fixed depth budget. As shown in Figure 8(a), allocating sufficient capacity to temporal modeling is essential, while excessive cross-variate routing significantly degrades performance. This indicates that robust temporal modeling is the foundation of forecasting, while cross-variate interaction provides complementary gains. **Falcon-X** achieves the best trade-off with a balanced 16/16 configuration.

Latent Prototype Dimension (C). We evaluate the representational capacity of the unified semantic space by varying C . Figure 8(b) demonstrates that a severely restricted dimension ($C \leq 2$) induces an information bottleneck, leading to semantic over-compression. Conversely, expanding the dimension enhances relational expressivity. The model achieves peak accuracy at $C = 6$ and $C = 8$, striking a perfect balance between capturing diverse dynamics and avoiding redundant noise.

5.5 Scaling Analysis

We evaluate the scaling behaviors of **Falcon-X** across training iterations and parameter sizes. As shown in Figure 6, the training dynamics exhibit a smooth, stable loss descent alongside continuous forecasting performance gains throughout the entire 1×10^6 steps. Furthermore, scaling the model capacity from 59M ($l = n = 8, D = 512$) to 253M ($l = n = 12, D = 768$) and up to 591M ($l = n = 16, D = 1024$) yields strictly predictable improvements in both MASE and CRPS (Figure 8(c)). These consistent trajectories demonstrate that our decoupled architecture strictly adheres to neural scaling laws, confirming its robust scalability and vast capacity to absorb massive heterogeneous time series without saturation.

5.6 Case Study

To qualitatively analyze **Falcon-X**, we present representative forecasting cases from GIFT-Eval.

Multivariate vs. Univariate Inference. We compare multivariate inference with channel-independent inference on highly correlated sequences from ETT1/15T (see Figure 9). Without cross-variate interactions, the channel-independent setting gradually drifts from the ground truth under complex temporal shifts. In contrast, **Falcon-X** leverages its unified latent prototype space to aggregate complementary signals across variates, producing substantially more accurate trajectories.

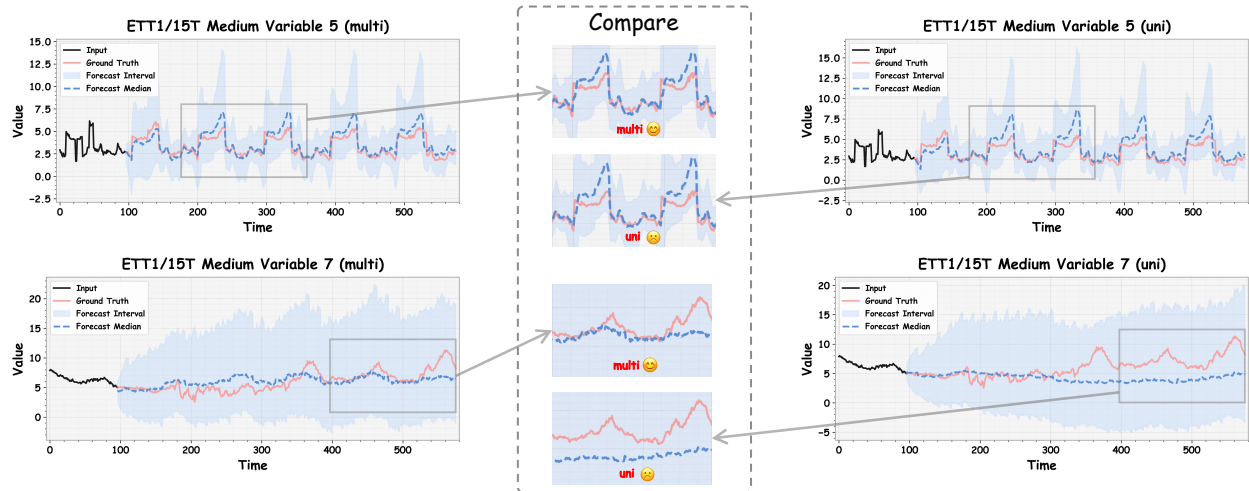


Figure 9 Case study on ETT1/15T dataset. In univariate inference mode, forecasts gradually deviate from the ground truth due to the absence of global context. In contrast, **Falcon-X**'s multivariate inference effectively leverages cross-variate signals to calibrate trajectories.

Positive and Negative Dependency Modeling. We further examine the ability of **Falcon-X** to capture dual dependencies. As shown in Figure 13, **Falcon-X** accurately models positive correlations with synchronized trends. More importantly, in Figure 14, it successfully captures negative correlations with opposing dynamics. These results validate the effectiveness of our Unified Prototype Diff-Attention for modeling both synergistic and antagonistic relationships.

6 Conclusion

In this paper, we identify two fundamental challenges of existing multivariate time series foundation models: semantic alignment and relational expressivity. To address these issues, we propose **Falcon-X**, a novel modeling paradigm that decouples physical variables into a unified latent prototype space. By introducing the Unified Prototype Diff-Attention, our architecture effectively captures both synergistic and antagonistic correlations. Additionally, a Variate Reassembly Router ensures robust global context fusion across diverse domains. Extensive evaluations on GIFT-Eval and fev-bench demonstrate that **Falcon-X** achieves state-of-the-art performance, showcasing exceptional scalability and zero-shot transferability. We hope that this work will contribute to the development of more unified and expressive foundation models for time series.

References

- Walmart Competition Admin and Will Cukierski. Walmart recruiting - store sales forecasting. <https://kaggle.com/competitions/walmart-recruiting-store-sales-forecasting>, 2014. Kaggle.
- Taha Aksu, Gerald Woo, Juncheng Liu, Xu Liu, Chenghao Liu, Silvio Savarese, Caiming Xiong, and Doyen Sahoo. Gift-EVAL: A benchmark for general time series forecasting model evaluation. *arXiv preprint arXiv:2410.10393*, 2024.
- Abdul Fatir Ansari, Lorenzo Stella, Caner Turkmen, Xiyuan Zhang, Pedro Mercado, Huibin Shen, Oleksandr Shchur, Syama Sundar Rangapuram, Sebastian Pineda Arango, Shubham Kapoor, et al. Chronos: Learning the language of time series. *Transactions on Machine Learning Research*, 2024.
- Abdul Fatir Ansari, Oleksandr Shchur, Jaris Küken, Andreas Auer, Boran Han, Pedro Mercado, Syama Sundar Rangapuram, Huibin Shen, Lorenzo Stella, Xiyuan Zhang, Mononito Goswami, Shubham Kapoor, Danielle C. Maddix, Pablo Guerron, Tony Hu, Junming Yin, Nick Erickson, Prateek Mutalik Desai, Hao Wang, Huzefa Rangwala, George Karypis, Yuyang Wang, and Michael Bohlke-Schneider. Chronos-2: From univariate to universal forecasting. *arXiv preprint arXiv:2510.15821*, 2025.
- George Athanasopoulos, Roman A. Ahmed, and Rob J. Hyndman. Hierarchical forecasts for Australian domestic tourism. *International Journal of Forecasting*, 25(1):146–166, January 2009. ISSN 0169-2070. doi: 10.1016/j.ijforecast.2008.07.004. <http://dx.doi.org/10.1016/j.ijforecast.2008.07.004>.
- Andreas Auer, Patrick Podest, Daniel Klotz, Sebastian Böck, Günter Klambauer, and Sepp Hochreiter. Tirez: Zero-shot forecasting across long and short horizons with enhanced in-context learning. In *Neural Information Processing Systems*, 2025.
- Jimmy Lei Ba, Jamie Ryan Kiros, and Geoffrey E Hinton. Layer normalization. In *arXiv preprint arXiv:1607.06450*, 2016.
- Lawrence J. Christiano, Martin Eichenbaum, and Charles L. Evans. Monetary policy shocks: What have we learned and to what end? In *Handbook of Macroeconomics*, volume 1 of *Handbook of Macroeconomics*, pages 65–148. Elsevier, 1999. doi: [https://doi.org/10.1016/S1574-0048\(99\)01005-8](https://doi.org/10.1016/S1574-0048(99)01005-8). <https://www.sciencedirect.com/science/article/pii/S1574004899010058>.
- Ben Cohen, Emaad Khwaja, Youssef Doubli, Salahidine Lemaachi, Chris Lettieri, Charles Masson, Hugo Miccinilli, Elise Ramé, Qiqi Ren, Afshin Rostamizadeh, et al. This time is different: An observability perspective on time series foundation models. In *Neural Information Processing Systems*, 2025.
- Abhimanyu Das, Weihao Kong, Rajat Sen, and Yichen Zhou. A decoder-only foundation model for time-series forecasting. In *International Conference on Machine Learning*, pages 10148–10167, 2024.
- Open Power System Data. Data package time series. version 2020-10-06, 2020. https://doi.org/10.25832/time_series/2020-10-06.
- UK COVID-19 data from official UK government sources. UK COVID-19 dashboard data. <https://www.kaggle.com/datasets/happyadam73/uk-covid19-dashboard-data-sqlite-compressed>, 2022. Kaggle.
- Etienne David, Jean Bellot, and Sylvain Le Corff. HERMES: Hybrid error-corrector model with inclusion of external signals for nonstationary fashion time series. *arXiv preprint arXiv:2202.03224*, 2022.
- S. De Vito, E. Massera, M. Piga, L. Martinotto, and G. Di Francia. On field calibration of an electronic nose for benzene estimation in an urban pollution monitoring scenario. *Sensors and Actuators B: Chemical*, 129(2):750–757, 2008. ISSN 0925-4005. doi: <https://doi.org/10.1016/j.snb.2007.09.060>. <https://www.sciencedirect.com/science/article/pii/S0925400507007691>.
- ECDC. Respiratory viruses weekly data. https://github.com/EU-ECDC/Respiratory_viruses_weekly_data/tree/main, 2025. Open data repository; weekly respiratory virus surveillance in the EU/EEA.
- Philip J Fleming and John J Wallace. How not to lie with statistics: the correct way to summarize benchmark results. *Communications of the ACM*, 29(3):218–221, 1986.
- FlorianKnauer and Will Cukierski. Rossmann store sales. <https://kaggle.com/competitions/rossmann-store-sales>, 2015. Kaggle.
- Rakshitha Wathsadini Godahewa, Christoph Bergmeir, Geoffrey I. Webb, Rob Hyndman, and Pablo Montero-Manso. Monash time series forecasting archive. In *The Conference on Neural Information Processing Systems Datasets and Benchmarks Track*, 2021. <https://openreview.net/forum?id=wEc1mgAJU->.

- Mononito Goswami, Konrad Szafer, Arjun Choudhry, Yifu Cai, Shuo Li, and Artur Dubrawski. MOMENT: A family of open time-series foundation models. In *International Conference on Machine Learning*, 2024.
- Tao Hong, Pierre Pinson, and Shu Fan. Global energy forecasting competition 2012. *International Journal of Forecasting*, 30(2):357–363, 2014.
- Shi Bin Hoo, Samuel Müller, David Salinas, and Frank Hutter. From tables to time: Extending tabPFN-v2 to time series forecasting. *arXiv preprint arXiv:2501.02945*, 2025.
- Addison Howard, Haruka Yui, Mark McDonald, and Will Cukierski. Recruit restaurant visitor forecasting. <https://www.kaggle.com/c/recruit-restaurant-visitor-forecasting>, 2017a. Kaggle.
- Addison Howard, Haruka Yui, Mark McDonald, and Will Cukierski. Recruit restaurant visitor forecasting. <https://kaggle.com/competitions/recruit-restaurant-visitor-forecasting>, 2017b. Kaggle.
- Jiawei Jiang, Chengkai Han, Wenjun Jiang, Wayne Xin Zhao, and Jingyuan Wang. Libcity: A unified library towards efficient and comprehensive urban spatial-temporal prediction. *arXiv preprint arXiv:2304.14343*, 2023.
- Ming Jin, Shiyu Wang, Lintao Ma, Zhixuan Chu, James Y Zhang, Xiaoming Shi, Pin-Yu Chen, Yuxuan Liang, Yuan-Fang Li, Shirui Pan, et al. Time-LLM: Time series forecasting by reprogramming large language models. In *International Conference on Learning Representations*, 2023.
- Emaad Khwaja, Chris Lettieri, Gerald Woo, Eden Belouadah, Marc Cenac, Guillaume Jarry, Enguerrand Paquin, Xunyi Zhao, Viktoriya Zhukov, Othmane Abou-Amal, et al. Toto 2.0: Time series forecasting enters the scaling era. *arXiv preprint arXiv:2605.20119*, 2026.
- Xiangjie Kong, Zhenghao Chen, Weiyao Liu, Kaili Ning, Lechao Zhang, Syaueqie Muhammad Marier, Yichen Liu, Yuhao Chen, and Feng Xia. Deep learning for time series forecasting: a survey. *International Journal of Machine Learning and Cybernetics*, 16(7):5079–5112, 2025.
- Siva Rama Krishna Kottapalli, Karthik Hubli, Sandeep Chandrashekhara, Garima Jain, Sunayana Hubli, Gayathri Botla, and Ramesh Daddaiah. Foundation models for time series: A survey. *arXiv preprint arXiv:2504.04011*, 2025.
- Guokun Lai, Wei-Cheng Chang, Yiming Yang, and Hanxiao Liu. Modeling long- and short-term temporal patterns with deep neural networks. In *The International ACM SIGIR Conference on Research & Development in Information Retrieval*, 2017. <https://api.semanticscholar.org/CorpusID:4922476>.
- lexis Cook, DanB, inversion, and Ryan Holbrook. Store sales – time series forecasting. <https://www.kaggle.com/competitions/store-sales-time-series-forecasting>, 2020. Kaggle.
- Chenghao Liu, Taha Aksu, Juncheng Liu, Xu Liu, Hanshu Yan, Quang Pham, Silvio Savarese, Doyen Sahoo, Caiming Xiong, and Junnan Li. Moirai 2.0: When less is more for time series forecasting. *arXiv preprint arXiv:2511.11698*, 2025a.
- Yong Liu, Haoran Zhang, Chenyu Li, Xiangdong Huang, Jianmin Wang, and Mingsheng Long. Timer: generative pre-trained transformers are large time series models. In *International Conference on Machine Learning*, pages 32369–32399, 2024.
- Yong Liu, Guo Qin, Zhiyuan Shi, Zhi Chen, Caiyin Yang, Xiangdong Huang, Jianmin Wang, and Mingsheng Long. Sundial: A family of highly capable time series foundation models. In *International Conference on Machine Learning*, pages 39295–39317. PMLR, 2025b.
- Yong Liu, Xingjian Su, Shiyu Wang, Haoran Zhang, Haixuan Liu, Yuxuan Wang, Zhou Ye, Yang Xiang, Jianmin Wang, and Mingsheng Long. Timer-S1: A billion-scale time series foundation model with serial scaling. *arXiv preprint arXiv:2603.04791*, 2026.
- Ilya Loshchilov and Frank Hutter. Decoupled weight decay regularization. In *International Conference on Learning Representations*, 2019. <https://openreview.net/forum?id=Bkg6RiCqY7>.
- Spyros Makridakis, Evangelos Spiliotis, and Vassilios Assimakopoulos. The M4 competition: Results, findings, conclusion and way forward. *International Journal of Forecasting*, 2018.
- Spyros Makridakis, Evangelos Spiliotis, and Vassilios Assimakopoulos. M5 accuracy competition: Results, findings, and conclusions. *International Journal of Forecasting*, 38(4):1346–1364, 2022. ISSN 0169-2070. doi: <https://doi.org/10.1016/j.ijforecast.2021.11.013>. <https://www.sciencedirect.com/science/article/pii/S0169207021001874>. Special Issue: M5 competition.
- Paolo Mancuso, Veronica Piccialli, and Antonio M Sudoso. A machine learning approach for forecasting hierarchical time series. *Expert Systems with Applications*, 182:115102, 2021.

- AI Maverick. Renewable energy and weather conditions. <https://www.kaggle.com/datasets/samanemami/renewable-energy-and-weather-conditions>, 2025. Kaggle.
- Michael W. McCracken and Serena Ng. FRED-MD: A monthly database for macroeconomic research. *Journal of Business & Economic Statistics*, 34(4):574–589, 2016. doi: 10.1080/07350015.2015.1086655. <https://doi.org/10.1080/07350015.2015.1086655>.
- Michael W. McCracken and Serena Ng. FRED-QD: A quarterly database for macroeconomic research. *Review*, 103(1): 1–44, January 2021. doi: 10.20955/r.103.1-44. <https://ideas.repec.org/a/fip/fedlrv/90588.html>.
- MichalKecera. Rohlik sales forecasting challenge. <https://kaggle.com/competitions/rohlik-sales-forecasting-challenge-v2>, 2024. Kaggle.
- Kamiar Mohaddes and Mehdi Raissi. Compilation, revision and updating of the global var (gvar) database. Mendeley Data, Version 1, 2024. <https://doi.org/10.17632/kfp5fhgkvf.1>.
- Yuqi Nie, Nam H Nguyen, Phanwadee Sinthong, and Jayant Kalagnanam. A time series is worth 64 words: Long-term forecasting with transformers. In *International Conference on Learning Representations*, 2023.
- Nafay Un Noor. Global life expectancy data (1950–2023). <https://www.kaggle.com/datasets/nafayunnoor/global-life-expectancy-data-1950-2023>, 2025. Kaggle.
- General Directorate of Health Affairs and Saudi Arabia Ministry of Health. Riyadh hospital admissions dataset (2020–2024). <https://www.kaggle.com/dsv/9992619>, 2024.
- Santosh Palaskar, Vijay Ekambaram, Arindam Jati, Neelamadhav Gantayat, Avirup Saha, Seema Nagar, Nam Nguyen, Pankaj Dayama, Renuka Sindhgatta, Prateeti Mohapatra, Harshit Kumar, Jayant Kalagnanam, Nandyala Hemachandra, and Narayan Rangaraj. Automixer for improved multivariate time-series forecasting on business and it observability data. *Proceedings of the AAAI Conference on Artificial Intelligence*, 38:22962–22968, 2024.
- Ulrik Thyge Pedersen. CO2 emissions by country. <https://www.kaggle.com/datasets/ulrikthygepedersen/co2-emissions-by-country>, 2025. Kaggle.
- Bushra Qurban. Tourism and economic impact. <https://www.kaggle.com/datasets/bushraqurban/tourism-and-economic-impact>, 2025. Kaggle.
- Oleksandr Shchur, Abdul Fatir Ansari, Caner Turkmen, Lorenzo Stella, Nick Erickson, Pablo Guerron, Michael Bohlke-Schneider, and Yuyang Wang. fev-bench: A realistic benchmark for time series forecasting. *arXiv preprint arXiv:2509.26468*, 2025.
- Siqi Shen, Vincent Van Beek, and Alexandru Iosup. Statistical characterization of business-critical workloads hosted in cloud datacenters. In *IEEE/ACM International Symposium on Cluster, Cloud and Grid Computing*, pages 465–474. IEEE, 2015.
- Mohammad Shoeybi, Mostofa Patwary, Raul Puri, Patrick LeGresley, Jared Casper, and Bryan Catanzaro. Megatron-LM: Training multi-billion parameter language models using model parallelism. *arXiv preprint arXiv:1909.08053*, 2019.
- Iain Staffell, Stefan Pfenninger, and Nathan Johnson. A global model of hourly space heating and cooling demand at multiple spatial scales. *Nature Energy*, 8(12):1328–1344, 2023. doi: 10.1038/s41560-023-01341-5. <https://doi.org/10.1038/s41560-023-01341-5>.
- Artur Trindade. ElectricityLoadDiagrams20112014. UCI Machine Learning Repository, 2015. DOI: <https://doi.org/10.24432/C58C86>.
- Alexander van Renen, Dominik Horn, Pascal Pfeil, Kapil Vaidya, Wenjian Dong, Murali Narayanaswamy, Zhengchun Liu, Gaurav Saxena, Andreas Kipf, and Tim Kraska. Why TPC is not enough: An analysis of the amazon redshift fleet. *Proc. VLDB Endow.*, 17(11):3694–3706, July 2024. ISSN 2150-8097. doi: 10.14778/3681954.3682031. <https://doi.org/10.14778/3681954.3682031>.
- Ashish Vaswani, Noam Shazeer, Niki Parmar, Jakob Uszkoreit, Llion Jones, Aidan N Gomez, Łukasz Kaiser, and Illia Polosukhin. Attention is all you need. *Advances in neural information processing systems*, 30, 2017.
- Jingyuan Wang, Jiawei Jiang, Wenjun Jiang, Chengkai Han, and Wayne Xin Zhao. Towards efficient and comprehensive urban spatial-temporal prediction: A unified library and performance benchmark. *arXiv preprint arXiv:2304.14343*, 2023.

- Ines Wilms and Christophe Croux. Forecasting using sparse cointegration. *International Journal of Forecasting*, 32(4): 1256–1267, 2016. ISSN 0169-2070. doi: <https://doi.org/10.1016/j.ijforecast.2016.04.005>. <https://www.sciencedirect.com/science/article/pii/S0169207016300589>.
- Gerald Woo, Chenghao Liu, Akshat Kumar, Caiming Xiong, Silvio Savarese, and Doyen Sahoo. Unified training of universal time series forecasting transformers. In *International Conference on Machine Learning*, 2024.
- Haixu Wu, Jiehui Xu, Jianmin Wang, and Mingsheng Long. Autoformer: Decomposition transformers with auto-correlation for long-term series forecasting. In *Neural Information Processing Systems*, 2021. <https://api.semanticscholar.org/CorpusID:235623791>.
- Shi Xiaoming, Wang Shiyu, Nie Yuqi, Li Dianqi, Ye Zhou, Wen Qingsong, and Ming Jin. Time-MoE: Billion-scale time series foundation models with mixture of experts. In *International Conference on Learning Representations*, 2025.
- Jiyuan Xu, Wenyu Zhang, Xin Jing, Jiahao Nie, Shuai Chen, and Shuai Zhang. CPiRi: Channel permutation-invariant relational interaction for multivariate time series forecasting. In *The International Conference on Learning Representations*, 2026. <https://openreview.net/forum?id=tgnXCCjKE3>.
- Siqiao Xue, Zhaoyang Zhu, Wei Zhang, Rongyao Cai, Rui Wang, Yixiang Mu, Fan Zhou, Jianguo Li, Peng Di, and Hang Yu. QuitoBench: A high-quality open time series forecasting benchmark. *arXiv preprint arXiv:2603.26017*, 2026.
- Tianzhu Ye, Li Dong, Yuqing Xia, Yutao Sun, Yi Zhu, Gao Huang, and Furu Wei. Differential transformer. In *International Conference on Learning Representations*, 2025.
- Haoyi Zhou, Shanghang Zhang, Jieqi Peng, Shuai Zhang, Jianxin Li, Hui Xiong, and Wancai Zhang. Informer: Beyond efficient transformer for long sequence time-series forecasting. In *Proceedings of the AAAI conference on artificial intelligence*, volume 35, pages 11106–11115, 2021.
- Jingbo Zhou, Xinjiang Lu, Yixiong Xiao, Jian Tang, Jiantao Su, Yu Li, Ji Liu, Junfu Lyu, Yanjun Ma, and Dejing Dou. SDWPF: A dataset for spatial dynamic wind power forecasting over a large turbine array. *Scientific Data*, 11(1):649, 2024. doi: [10.1038/s41597-024-03427-5](https://doi.org/10.1038/s41597-024-03427-5). <https://doi.org/10.1038/s41597-024-03427-5>.

A Methodology Design Philosophies

A.1 Overall Architecture

As shown in Figure 2, the architecture of **Falcon-X** follows a hierarchical transformation pipeline that progressively aligns heterogeneous variates into a unified latent space, and ultimately reconstructs them for accurate forecasting. We formulate the forecasting task as a unified masked reconstruction paradigm. Formally, the input heterogeneous series $\mathbf{X} \in \mathbb{R}^{M \times (L+T)}$ is first subjected to instance normalization and tokenization to generate the time tokens $\mathbf{H} \in \mathbb{R}^{M \times P \times D}$, where $P = \frac{L+T}{L_p}$ is the number of patches and L_p is the length of patches. These tokens are then processed through time attention layers, yielding temporal representations $\mathbf{H}_T \in \mathbb{R}^{M \times P \times D}$.

To bridge the dimensionality gap, **Falcon-X** employs the Unified Prototype Diff-Attention (UPDA) to project the disparate N entities into a compact, unified prototype space $\mathbf{H}_C \in \mathbb{R}^{(N \times P) \times C \times D}$. Following cross-variate interactions via Latent Entity Attention (LEA), which yields the refined context \mathbf{H}'_C , the Variate Reassembly Router (VRR) performs a soft-routing operation to retrieve and reassemble the latent representations back into the entity-specific space $\mathbf{H}_V \in \mathbb{R}^{M \times P \times D}$ by matching the routing request in \mathbf{H}_T with the prototype index in \mathbf{H}'_C .

Finally, the reassembled entities \mathbf{H}_V are fused with the temporal representations \mathbf{H}_T and mapped through a quantile forecasting head to produce the final predictive output $\hat{\mathbf{Y}} \in \mathbb{R}^{M \times T}$, completing the end-to-end flow from raw heterogeneous inputs to unified latent representations and back to structured forecasts.

A.2 Time Attention

To capture the intrinsic evolutionary patterns of each individual variate, **Falcon-X** utilizes an encoder-only Transformer architecture. A critical design choice in **Falcon-X** is the deliberate decoupling of temporal and cross-variate modeling. Unlike many existing multivariate models, which interleave temporal and spatial mixing, leading to semantic entanglement whereby a variate’s subtle temporal signal is prematurely confounded by the noisy dependencies of its heterogeneous neighbors, **Falcon-X** prioritizes establishing a robust temporal module. Stacking n layers of Time Attention before any cross-variate interaction ensures that the temporal evolutive state of each variate is fully distilled and stabilised. This provides a clean, time-aware foundation for the subsequent Variate Attention process.

A.3 Variate Attention

A core requirement of time-series foundation models is *the ability to transcend rigid, dataset-specific dimensional constraints and learn a unified representation of dependencies across multivariate series*. However, treating different physical variates homogeneously or simply concatenating them leads to severe semantic misalignment. To overcome this, **Falcon-X** introduces a unified latent space paradigm. As shown in Figure 2(a–c), these modules progressively aligns the heterogeneous patch embeddings \mathbf{H}_T into a shared prototype space, models both intra- and cross-dataset dependencies, and dynamically reassembles the global context back to the original variate dimensions.

A.3.1 Unified Prototype Diff-Attention

The primary challenge in modeling the foundations of time series lies in reconciling diverse physical variates within a unified semantic space. Dataset-level group mixing (Ansari et al., 2025) relies on

dense intra-dataset attention, lacking structural abstraction and incurring quadratic complexity $\mathcal{O}(M^2)$. To address this, **Falcon-X** introduces prototype alignment, projecting heterogeneous variates into a fixed set of learnable latent temporal prototypes of dimension C .

Instead of relying on arbitrary physical indexing, this paradigm dynamically allocates the full representation of each independent variate across the C universal prototypes based on their intrinsic semantic affinity, thereby achieving explicit semantic unification. This explicit mapping resolves the issue of semantic misalignment by aligning variates with similar temporal dynamics to the same semantic anchors, regardless of their original dataset or spatial proximity. Furthermore, by forcing the representations through this fixed-dimensional prototype space, the model inherently performs structural denoising, filtering out localized noise and isolating the most salient temporal patterns. Importantly, this projection replaces dense intra-dataset attention with cross-attention, decoupling the computational bottleneck from the physical dimensionality. The complexity is thus reduced to a strictly linear $\mathcal{O}(M \cdot C)$, effortlessly accommodating extreme-dimensional modeling since $C \ll M$.

Furthermore, we observe that negative correlations among heterogeneous variates, which are critical for capturing counteracting interactions across diverse time series, are difficult to exploit in standard Transformer architectures. This limitation stems from the non-negative nature of the softmax attention function, which restricts attention scores to the range $[0, 1]$ and thus prevents the explicit modeling of opposing trends. To address this, we draw inspiration from differential attention (Ye et al., 2025). While originally proposed for attention noise suppression, **Falcon-X** repurposes this mechanism to capture dual-dependency dynamics. By introducing positive and negative learnable keys, the model explicitly represents both synergistic and antagonistic relationships, yielding improved expressiveness of the cross-variate latent space.

A.3.2 Latent Entity Attention

Following the alignment of heterogeneous variates into the unified prototype space, this module models the comprehensive interactions among different variates. As all representations now reside in a shared, dimension-agnostic semantic space rather than their original disparate physical dimensions, Latent Entity Attention naturally facilitates cross-learning. This enables **Falcon-X** to leverage and transfer shared structural patterns across entirely different domains, thereby significantly enhancing zero-shot cross-dataset generalization.

A.3.3 Variate Reassembly Router

After capturing comprehensive dependencies in the unified prototype space, the model must reassemble this global context back into the original heterogeneous dimensions (m_i). **Falcon-X** formulates this reassembly as a targeted retrieval from the abstract prototype space to individual variate trajectories. The aim is to reconstruct the heterogeneous variates, each with distinct temporal patterns, by retrieving relevant information from the unified latent prototypes.

This is orchestrated via a *request-and-dispatch* mechanism: the Routing Request (\mathbf{R}_{req}), derived from \mathbf{h}_T^i , acts as a structural query conveying the specific physical dimensionality and unique temporal trajectory of the original variate, effectively serving as *entity identity tag*. The request is then matched against the Prototype Index (\mathbf{P}_{idx}), which is an addressable map of the global prototype library. Meanwhile, the Source Context (\mathbf{S}_{ctx}) delivers the refined semantic payloads. Using local, specific trajectories to selectively retrieve unified global prototypes enables this routing paradigm to reconstruct variate-specific patterns with high fidelity.

Finally, considering the significant variance in cross-variate dependencies across diverse datasets, forcing a uniform integration of the global context could introduce detrimental noise to datasets with inherently weak variate correlations. To maintain strict cross-dataset robustness, we introduce an explicit gated residual connection to dynamically fuse the temporal embeddings \mathbf{H}_T with the cross-variate representations \mathbf{H}_V . Consequently, it effectively prevents semantic interference in weakly correlated systems while making full use of cross-variate dependencies in strongly correlated ones.

B Dataset Statistics

This section summarizes the datasets used in our experiments. Specifically, Appendix B.1 describes the corpus used for model pre-training, while Appendix B.2 and Appendix B.3 present the benchmarks used for downstream evaluation.

B.1 Pre-training Corpus

Our pre-training corpus comprises both **real-world** and **synthetic** time series datasets, covering a broad range of domains and data-generation characteristics.

Real-world datasets. We aggregate several large-scale time series collections, including the GIFT-EVAL (Aksu et al., 2024) pre-training dataset¹, the CHRONOS (Ansari et al., 2024) training corpus², and the QUITOBENCH (Xue et al., 2026) training dataset³, as detailed in Table 2. Collectively, these resources span seven major domains: *nature, energy, transport, finance, healthcare, web, and sales*. The resulting corpus contains a large number of *univariate* time series datasets, as well as a small set of *multivariate* time series datasets.

Synthetic univariate datasets. We also incorporate the synthetic *univariate* datasets introduced by CHRONOS (Ansari et al., 2024): TSMIXUP and KERNELSYNTH. TSMIXUP synthesizes new time series by taking random convex combinations of samples drawn from different real-world datasets, thereby increasing diversity while preserving realistic temporal characteristics. KERNELSYNTH, in contrast, generates synthetic series by randomly composing Gaussian Process (GP) kernels and sampling from the resulting GP priors, producing time series with diverse trends, periodicities, and stochastic patterns.

Synthetic multivariate datasets. High-quality *multivariate* time series datasets remain relatively scarce in existing public resources. To address this limitation, we construct a large amount of synthetic *multivariate* data through two complementary strategies:

1. **Similarity-based multivariate construction from real univariate series.** Drawing from the real univariate time series presented in Table 2, we compute pairwise similarities to group related sequences into cohesive multivariate datasets. This process enables us to derive multivariate structures from naturally occurring signals while preserving semantic coherence across dimensions.
2. **Dependency injection over synthetic univariate generators.** Inspired by Chronos-2 (Ansari et al., 2025), we transform multiple independently sampled univariate series from base generators (e.g., KERNELSYNTH) into multivariate synthetic time series by imposing explicit dependency structures. These multivariate construction procedures include:

¹<https://huggingface.co/datasets/Salesforce/GiftEvalPretrain>

²https://huggingface.co/datasets/autogluon/chronos_datasets

³<https://huggingface.co/datasets/hq-bench/quito-corpus>

Table 2 Summary statistics of univariate pre-training datasets.

Dataset Name	Frequency	Time Series	Variates	Time Points	Domain	Source
BDG-2	H	611	1	9,454,968	Energy	GIFT-Eval
BEIJING_SUBWAY_30MIN	30T	276	2	433,872	Transport	GIFT-Eval
CIF 2016	M	72	1	6,334	Finance	GIFT-Eval
CMIP6	6H	270,336	53	1,973,452,800	Nature	GIFT-Eval
ERA5	H	245,760	45	2,146,959,360	Nature	GIFT-Eval
Electricity	H, W	642	1	8,493,660	Energy	Chronos
HZMETRO	15T	80	2	190,160	Transport	GIFT-Eval
LOS_LOOP	5T	207	1	7,094,304	Transport	GIFT-Eval
LargeST	5T	42,333	1	4,452,510,528	Transport	GIFT-Eval
M1	A, M, Q	921	1	57,882	Finance	GIFT-Eval
M3	A, M, Q	3,003	1	209,114	Finance	GIFT-Eval
NN5	D, W	222	1	93,240	Finance	GIFT-Eval
PEMS03	5T	358	1	9,382,464	Transport	GIFT-Eval
PEMS04	5T	307	3	5,216,544	Transport	GIFT-Eval
PEMS07	5T	883	1	24,921,792	Transport	GIFT-Eval
PEMS08	5T	170	3	3,035,520	Transport	GIFT-Eval
PEMS_BAY	5T	325	1	16,941,600	Transport	GIFT-Eval
Q-TRAFFIC	15T	45,148	1	264,386,688	Transport	GIFT-Eval
Quito	10T, H	33,806	5	313,269,828	Various	QuitoBench
Residential Power	T	504	3	271,333,509	Energy	GIFT-Eval
SHMETRO	15T	288	2	2,536,992	Transport	GIFT-Eval
Solar	5T, H	10,332	1	588,304,080	Energy	Chronos
Taxi	30T, H	70,412	1	56,793,348	Transport	Chronos
Tourism	A, M, Q	1,212	1	150,822	Finance	GIFT-Eval
Traffic	H, W	1,724	1	15,060,864	Transport	GIFT-Eval
Uber TLC	D, H	524	1	1,176,531	Transport	GIFT-Eval
Weatherbench	D, H, W	675,840	1	82,753,646,592	Nature	Chronos
Wind Farms	D, H, T	1,011	1	175,154,333	Energy	Chronos
alibaba_cluster_trace_2018	5T	58,409	2	95,192,530	Web	GIFT-Eval
australian_electricity_demand	30T	5	1	1,153,584	Energy	GIFT-Eval
azure_vm_traces_2017	5T	159,472	1	885,522,908	Web	GIFT-Eval
beijing_air_quality	H	12	11	420,768	Nature	GIFT-Eval
bitcoin_with_missing	D	18	1	81,918	Finance	GIFT-Eval
borealis	H	15	1	83,269	Energy	GIFT-Eval
borg_cluster_data_2011	5T	143,386	2	537,552,854	Web	GIFT-Eval
buildings_900k	H	1,792,328	1	15,702,585,608	Energy	GIFT-Eval
bull	H	41	1	719,304	Energy	GIFT-Eval
cdc_fluview_ilinet	W	75	5	63,903	Healthcare	GIFT-Eval
cdc_fluview_who_nrevss	W	74	4	41,760	Healthcare	GIFT-Eval
china_air_quality	H	437	6	5,739,234	Nature	GIFT-Eval
cockatoo	H	1	1	17,544	Energy	GIFT-Eval
covid19_energy	H	1	1	31,912	Energy	GIFT-Eval
covid_mobility	D	362	1	148,602	Transport	GIFT-Eval
dominick	W	100,014	1	29,652,492	Sales	Chronos
elecdemand	30T	1	1	17,520	Energy	GIFT-Eval
elf	H	1	1	21,792	Energy	GIFT-Eval
exchange_rate	D	8	1	84,976	Finance	Chronos
extended_web_traffic_with_missing	D	145,063	1	370,926,091	Web	GIFT-Eval
godaddy	M	3,135	2	128,535	Finance	GIFT-Eval
hog	H	24	1	421,056	Energy	GIFT-Eval
ideal	H	217	1	1,255,253	Energy	GIFT-Eval
kaggle_web_traffic_weekly	W	145,063	1	16,537,182	Web	GIFT-Eval
lcl	H	713	1	9,543,553	Energy	GIFT-Eval
london_smart_meters_with_missing	30T	5,520	1	166,238,880	Energy	GIFT-Eval
mexico_city_bikes	H	494	1	38,687,004	Transport	Chronos
oikolab_weather	H	8	1	800,456	Nature	GIFT-Eval
pdb	H	1	1	17,520	Energy	GIFT-Eval
pedestrian_counts	H	66	1	3,130,762	Transport	GIFT-Eval
project_tycho	W	1,258	1	1,377,707	Healthcare	GIFT-Eval
rideshare_with_missing	H	2,304	1	859,392	Transport	GIFT-Eval
sceaux	H	1	1	34,223	Energy	GIFT-Eval
smart	H	5	1	95,709	Energy	GIFT-Eval
solar_power	4S	1	1	7,397,222	Energy	GIFT-Eval
spain	H	1	1	35,064	Energy	GIFT-Eval
subseasonal	D	862	4	14,197,140	Nature	GIFT-Eval
subseasonal_precip	D	862	1	9,760,426	Nature	GIFT-Eval
sunspot_with_missing	D	1	1	73,894	Nature	GIFT-Eval
ushcn_daily	D	1,218	5	47,080,115	Nature	Chronos
vehicle_trips_with_missing	D	329	1	32,512	Transport	GIFT-Eval
weather	D	3,010	1	42,941,700	Nature	GIFT-Eval
wiki-rolling_nips	D	47,675	1	40,619,100	Web	GIFT-Eval
wiki_daily_100k	D	100,000	1	274,100,000	Web	Chronos
wind_power	4S	1	1	7,397,147	Energy	GIFT-Eval

Note. Frequency aliases follow common time-series conventions: S = second, T = minute, H = hourly, D = daily, W = weekly, M = monthly, Q = quarterly, and A = annual.

- **Cotemporaneous multivariatizers**, which introduce instantaneous cross-variate dependencies through linear or nonlinear transformations at the same time step;
- **Sequential multivariatizers**, which impose temporal cross-series relations across time, such as *lead-lag* dependencies and *cointegration*.

Through this combination of real-world corpora, *univariate* synthetic generators, and large-scale *multivariate* synthesis, our dataset collection supports training and evaluation across diverse domains and temporal dependency structures.

B.2 GIFT-Eval Benchmark

GIFT-Eval is constructed from 15 univariate and 8 multivariate datasets, spanning 7 domains and 10 frequencies. In total, the benchmark contains 144,000 time series and 177 million observations. To support evaluation across forecasting horizons, prediction lengths are determined in two ways. For widely used benchmarks such as M4 (Makridakis et al., 2018), established prediction lengths are retained. For the remaining datasets, the short-horizon prediction length is set to 48 time steps, and the medium- and long-horizon settings are defined according to dataset frequency and domain as $10\times$ and $15\times$ the short-horizon length, respectively. This results in 97 unique combinations of dataset, frequency, and prediction length, with model performance reported as the geometric mean across these configurations.

The benchmark is curated from 10 publicly available sources covering a diverse set of application domains. Below, the included datasets are grouped by domain and described together with their original sources.

- **Nature.** The benchmark includes the Jena Weather dataset⁴, following the preprocessing protocol used in **Autoformer** (Wu et al., 2021).
- **Web/CloudOps.** This domain contains the BizITObs Application, Service, and L2C datasets⁵, processed according to the pipeline introduced in **AutoMixer** (Palaskar et al., 2024). These datasets combine business KPIs with IT event channels, forming multivariate time series for observability-related forecasting tasks. In addition, Bitbrains datasets from the **Grid Workloads Archive** (Shen et al., 2015) are included in the same domain.
- **Sales.** For the sales domain, the Restaurant dataset is adopted from the **Recruit Restaurant Forecasting Competition** (Howard et al., 2017b), where the objective is to predict future customer visits using reservation and visitation records. Another sales dataset is included from Mancuso et al. (2021).
- **Energy.** The energy domain includes ETT1 and ETT2 from **Informer** (Zhou et al., 2021), which represent electricity transformer temperature and are widely used in long-horizon forecasting. It also includes the Electricity dataset from the **UCI ML Archive** (Trindade, 2015), containing electricity consumption records for 370 clients, and the Solar dataset from **LSTNet** (Lai et al., 2017), which focuses on forecasting solar plant power output.
- **Transport.** Transport datasets are drawn from **LibCity** (Wang et al., 2023), a benchmark collection of urban spatio-temporal and time series datasets.
- **Econ/Fin & Healthcare.** A subset of datasets is selected from the **Monash** repository (Godhewa et al., 2021), which provides a broad collection of time series from multiple domains.

⁴<https://www.bgc-jena.mpg.de/wetter/>

⁵<https://github.com/BizITObs/BizITObservabilityData/tree/main>

Table 3 Statistics of the GIFT-Eval benchmark across seven domains. Entries under Short-term/Med-term/Long-term are reported as Pred/Win, denoting the prediction length and the number of rolling windows, respectively.

Domain	Dataset Name	Freq.	#Series	Avg. length	#Vars	Short-term	Med-term	Long-term
Nature	Jena Weather	10T	1	52,704	21	48 / 20	480 / 11	720 / 8
		H	1	8,784	21	48 / 19	480 / 2	720 / 2
		D	1	366	21	30 / 2	-	-
	Saugeen	D	1	23,741	1	30 / 20	-	-
		W-THU	1	3,391	1	8 / 20	-	-
		M	1	780	1	12 / 7	-	-
	Temperature Rain	D	32,072	725	1	30 / 3	-	-
	KDD Cup 2018	H	270	10,898	1	48 / 20	480 / 2	720 / 2
D		270	455	1	30 / 2	-	-	
Web/CloudOps	BizITObs - Application	10S	1	8,834	2	60 / 15	600 / 2	900 / 1
	BizITObs - Service	10S	21	8,835	2	60 / 15	600 / 2	900 / 1
	BizITObs - L2C	5T	1	31,968	7	48 / 20	480 / 7	720 / 5
		H	1	2,664	7	48 / 6	480 / 1	720 / 1
	Bitbrains - Fast Storage	5T	1,250	8,640	2	48 / 18	480 / 2	720 / 2
		H	1,250	721	2	48 / 2	-	-
	Bitbrains - rnd	5T	500	8,640	2	48 / 18	480 / 2	720 / 2
		H	500	720	2	48 / 2	-	-
Energy	ETT1	15T	1	69,680	7	48 / 20	480 / 15	720 / 10
		H	1	17,420	7	48 / 20	480 / 4	720 / 3
		D	1	725	7	30 / 3	-	-
	ETT2	W-THU	1	103	7	8 / 2	-	-
		15T	1	69,680	7	48 / 20	480 / 15	720 / 10
		H	1	17,420	7	48 / 20	480 / 4	720 / 3
	Solar	D	1	725	7	30 / 3	-	-
		W-THU	1	103	7	8 / 2	-	-
		10T	137	52,560	1	48 / 20	480 / 11	720 / 8
	Electricity	H	137	8,760	1	48 / 19	480 / 2	720 / 2
		D	137	365	1	30 / 2	-	-
		W-FRI	137	52	1	8 / 1	-	-
	Electricity	15T	370	140,256	1	48 / 20	480 / 20	720 / 20
		H	370	35,064	1	48 / 20	480 / 8	720 / 5
		D	370	1,461	1	30 / 5	-	-
Electricity	W-FRI	370	208	1	8 / 3	-	-	
	Loop Seattle	5T	323	105,120	1	48 / 20	480 / 20	720 / 15
		H	323	8,760	1	48 / 19	480 / 2	720 / 2
D		323	365	1	30 / 2	-	-	
SZ-Taxi	15T	156	2,976	1	48 / 7	480 / 1	720 / 1	
	H	156	744	1	48 / 2	-	-	
M_DENSE	H	30	17,520	1	48 / 20	480 / 4	720 / 3	
	D	30	730	1	30 / 3	-	-	
Sales	Restaurant	D	807	358	1	30 / 1	-	-
	Hierarchical Sales	D	118	1,825	1	30 / 7	-	-
		W-WED	118	260	1	8 / 4	-	-
Car Parts	M	2,674	51	1	12 / 1	-	-	
Econ/Fin	M4 Yearly	A	22,974	37	1	6 / 1	-	-
	M4 Quarterly	Q	24,000	100	1	8 / 1	-	-
	M4 Monthly	M	48,000	234	1	18 / 1	-	-
	M4 Weekly	W	359	1,035	1	13 / 1	-	-
	M4 Daily	D	4,227	2,371	1	14 / 1	-	-
	M4 Hourly	H	414	902	1	48 / 2	-	-
Healthcare	Hospital	M	767	84	1	12 / 1	-	-
	COVID Deaths	D	266	212	1	30 / 1	-	-
	US Births	D	1	7,305	1	30 / 20	-	-
		W-TUE	1	1,043	1	8 / 14	-	-
		M	1	240	1	12 / 2	-	-

The selected datasets are chosen to avoid any leakage between pretraining and test data.

Detailed dataset statistics are provided in Table 3, including frequency, prediction length, variate setting, number of series, series length, and total number of observations. For each time series, the final 10% of observations is reserved as the test split.

B.3 fev-bench Benchmark

The fev-bench benchmark comprises a total of 100 time series forecasting tasks. Detailed dataset statistics are provided in Table 4. This section summarizes the main characteristics of these tasks and provides citations for the corresponding data sources. For datasets originating from forecasting competitions, the benchmark adopts the fixed forecast horizon T specified by the original competition setup. For all other datasets, the forecast horizon is determined according to a frequency–horizon mapping. An exception is made for a subset of hourly datasets, for which $T = 168$ is used in order to support long-range forecasting over a one-week period. The number of evaluation windows W is then selected so as to split each series as evenly as possible while ensuring that sufficient historical context remains available for every forecast of length H . Dataset frequencies are reported using pandas frequency aliases, namely `minutely`, `Hourly`, `Daily`, `Weekly`, `Monthly`, `Quarterly`, and `Yearly`.

The benchmark is constructed from a diverse collection of domains, including macroeconomics, energy systems, retail and sales forecasting, epidemiology, public health, environmental monitoring, and database operations. The included datasets can be grouped into the following source categories.

- **GIFT-Eval.** The benchmark includes datasets from the GIFT-Eval corpus (Aksu et al., 2024), which contains a mixture of univariate and multivariate forecasting tasks. The original GIFT-Eval collection draws on data sources compiled from prior benchmark and application papers (Godaheva et al., 2021; Jiang et al., 2023; Mancuso et al., 2021; Wu et al., 2021; Palaskar et al., 2024).
- **Macroeconomic datasets.** A broad set of macroeconomic and socioeconomic datasets is included, such as GVAR (Mohaddes and Raissi, 2024), US Consumption (Wilms and Croux, 2016), Australian Tourism (Athanasopoulos et al., 2009), FRED-MD (McCracken and Ng, 2016), FRED-QD (McCracken and Ng, 2021), world CO₂ emissions (Pedersen, 2025), life expectancy (Noor, 2025), and global tourism (Qurban, 2025). For both FRED-MD and FRED-QD, two separate forecasting tasks are defined. The first task follows the CEE model (Christiano et al., 1999) and focuses on forecasting employment, inflation, and federal funds rate indicators. The second task considers the joint forecasting of 51 core macroeconomic indicators. It should be noted that the benchmark uses the August 2025 snapshot of FRED-MD, which differs from the snapshot used in Monash repository (Godaheva et al., 2021).
- **Energy datasets.** The energy-related portion of the benchmark includes several forecasting settings of practical relevance. These datasets cover the electricity price forecasting (EPF) benchmark (Fleming and Wallace, 1986), ERCOT generation data (Ansari et al., 2024), ENTSO-e load data (Data, 2020) paired with weather variates obtained from Renewables.ninja (Staffell et al., 2023), and solar generation data (Maverick, 2025). Together, these datasets provide a mix of load, price, and renewable generation forecasting tasks.
- **BOOMLET.** The benchmark also includes multivariate observability datasets from BOOMLET (Cohen et al., 2025), which is itself a subset of the larger BOOM benchmark curated by the original authors. To maintain diversity across data sources and prevent overrepresentation

from a single benchmark family, only BOOMLET datasets with a sampling frequency of at least one minute are retained.

- **Forecasting competitions.** A substantial portion of the benchmark is drawn from forecasting competitions, many of which were hosted on kaggle.com. These include Favorita store sales and transactions (lexis Cook et al., 2020), the M5 competition (Makridakis et al., 2022), restaurant visitor and reservation forecasting (Howard et al., 2017a), Rossmann store sales (FlorianKnauer and Cukierski, 2015), Walmart sales forecasting (Admin and Cukierski, 2014), and Rohlik sales forecasting (MichalKecera, 2024). In addition, the benchmark includes the KDD Cup 2022 dataset for wind power forecasting (Zhou et al., 2024), as well as datasets from the Global Energy Forecasting Competitions held in 2012, 2014, and 2017 (Hong et al., 2014). These competition datasets typically come with standardized train–test setups and fixed forecast horizons, making them especially useful for controlled model comparison.
- **Other sources.** To further broaden domain coverage, the benchmark incorporates datasets from several additional sources:
 - Influenza-like illness case counts collected by the European Centre for Disease Prevention and Control (ECDC, 2025).
 - Fashion trend data from Hermes (David et al., 2022).
 - Hospital admissions data from Riyadh (of Health Affairs and Ministry of Health, 2024).
 - Query count data for Amazon Redshift database servers (van Renen et al., 2024).
 - Solar energy generation data with associated weather covariates (Maverick, 2025).
 - Air quality measurements from an Italian city together with weather variates (De Vito et al., 2008).
 - COVID-19 cases, hospital admissions, and deaths in the United Kingdom across multiple administrative levels (data from official UK government sources, 2022).

These additional datasets complement the benchmark by introducing forecasting tasks from healthcare, epidemiology, fashion, environmental sensing, and cloud/database system monitoring, thereby increasing the breadth of real-world scenarios represented in fev-bench.

Table 4 Individual statistics of the fev-bench benchmark across all datasets.

Task	Domain	Freq.	T	W	Median length	# series	# targets
GIFT-Eval							
BizTObs-L2C	cloud	5T	288	20	31,968	1	7
BizTObs-L2C	cloud	H	24	20	2,664	1	7
ETT	energy	15T	96	20	69,680	2	7
ETT	energy	H	168	20	17,420	2	7
ETT	energy	D	28	20	724	2	7
ETT	energy	W	13	5	103	2	7
Hierarchical Sales	retail	D	28	10	1,825	118	1
Hierarchical Sales	retail	W	13	10	260	118	1
Hospital	healthcare	M	12	4	84	767	1
Jena Weather	nature	10T	144	20	52,704	1	21
Jena Weather	nature	D	28	11	366	1	21
Jena Weather	nature	H	24	20	8,784	1	21
Loop Seattle	mobility	D	28	10	365	323	1
Loop Seattle	mobility	5T	288	10	105,120	323	1
Loop Seattle	mobility	H	168	10	8,760	323	1
M-DENSE	mobility	D	28	10	730	30	1
M-DENSE	mobility	H	168	10	17,520	30	1
SZ Taxi	mobility	15T	96	10	2,976	156	1
SZ Taxi	mobility	H	168	2	744	156	1

Continued on next page

Table 4 Individual statistics of the fev-bench benchmark across all datasets. (continued)

Task	Domain	Freq.	H	W	Median length	# series	# targets
Solar	energy	W	13	1	52	137	1
Solar	energy	D	28	10	365	137	1
Macroeconomic datasets							
Australian Tourism	econ	Q	8	2	36	89	1
FRED-MD-CEE	econ	M	12	20	798	1	3
FRED-MD-Macro	econ	M	12	20	798	1	51
FRED-QD-CEE	econ	Q	8	20	266	1	3
FRED-QD-Macro	econ	Q	8	20	266	1	51
GVAR	econ	Q	8	10	178	33	6
US Consumption	econ	M	12	10	792	31	1
US Consumption	econ	Q	8	10	262	31	1
US Consumption	econ	Y	5	10	64	31	1
World CO2 Emissions	econ	Y	5	9	60	191	1
World Life Expectancy	econ	Y	5	10	74	237	1
World Tourism	econ	Y	5	2	21	178	1
Energy datasets							
ENTSO-e Load	energy	15T	96	20	175,292	6	1
ENTSO-e Load	energy	30T	96	20	87,645	6	1
ENTSO-e Load	energy	H	168	20	43,822	6	1
EPF-BE	energy	H	24	20	52,416	1	1
EPF-DE	energy	H	24	20	52,416	1	1
EPF-FR	energy	H	24	20	52,416	1	1
EPF-NP	energy	H	24	20	52,416	1	1
EPF-PJM	energy	H	24	20	52,416	1	1
ERCOT	energy	D	28	20	6,452	8	1
ERCOT	energy	H	168	20	154,872	8	1
ERCOT	energy	M	12	15	211	8	1
ERCOT	energy	W	13	20	921	8	1
GFC12	energy	H	168	10	39,414	11	1
GFC14	energy	H	168	20	17,520	1	1
GFC17	energy	H	168	20	17,544	8	1
Solar with Weather	energy	15T	96	20	198,600	1	1
Solar with Weather	energy	H	24	20	49,648	1	1
BOOMLET							
BOOMLET-1062	cloud	5T	288	20	16,384	1	21
BOOMLET-1209	cloud	5T	288	20	16,384	1	53
BOOMLET-1225	cloud	T	60	20	16,384	1	49
BOOMLET-1230	cloud	5T	288	20	16,384	1	23
BOOMLET-1282	cloud	T	60	20	16,384	1	35
BOOMLET-1487	cloud	5T	288	20	16,384	1	54
BOOMLET-1631	cloud	30T	96	20	10,463	1	40
BOOMLET-1676	cloud	30T	96	20	10,463	1	100
BOOMLET-1855	cloud	H	24	20	5,231	1	52
BOOMLET-1975	cloud	H	24	20	5,231	1	75
BOOMLET-2187	cloud	H	24	20	5,231	1	100
BOOMLET-285	cloud	T	60	20	16,384	1	75
BOOMLET-619	cloud	T	60	20	16,384	1	52
BOOMLET-772	cloud	T	60	20	16,384	1	67
BOOMLET-963	cloud	T	60	20	16,384	1	28
Forecasting competitions							
Favorita Store Sales	retail	M	12	2	54	1,579	1
Favorita Store Sales	retail	W	13	10	240	1,579	1
Favorita Store Sales	retail	D	28	10	1,688	1,579	1
Favorita Transactions	retail	M	12	2	54	51	1
Favorita Transactions	retail	W	13	10	240	51	1
Favorita Transactions	retail	D	28	10	1,688	51	1
KDD Cup 2022	energy	D	14	10	243	134	1
KDD Cup 2022	energy	10T	288	10	35,279	134	1
KDD Cup 2022	energy	30T	96	10	11,758	134	1
M5	retail	M	12	1	58	30,490	1
M5	retail	W	13	1	257	30,490	1
M5	retail	D	28	1	1,810	30,490	1
Restaurant	retail	D	28	8	296	817	1
Rohlik Orders	retail	W	8	5	170	7	1
Rohlik Orders	retail	D	61	5	1,197	7	1
Rohlik Sales	retail	W	8	1	150	5,243	1
Rohlik Sales	retail	D	14	1	1,046	5,390	1
Rossmann	retail	W	13	8	133	1,115	1
Rossmann	retail	D	48	10	942	1,115	1
Walmart	retail	W	39	1	143	2,936	1
Other datasets							
ECDC ILI	healthcare	W	13	10	201	25	1

Continued on next page

Table 4 Individual statistics of the fev-bench benchmark across all datasets. (*continued*)

Task	Domain	Freq.	H	W	Median length	# series	# targets
Hermes	retail	W	52	1	261	10,000	1
Hospital Admissions	healthcare	D	28	20	1,731	8	1
Hospital Admissions	healthcare	W	13	16	246	8	1
Redset	cloud	5T	288	10	25,920	118	1
Redset	cloud	15T	96	10	8,640	126	1
Redset	cloud	H	24	10	2,160	138	1
UCI Air Quality	nature	H	168	20	9,357	1	4
UCI Air Quality	nature	D	28	11	389	1	4
UK COVID-Nation-Cumulative	healthcare	D	28	20	729	4	3
UK COVID-Nation-Cumulative	healthcare	W	8	4	105	4	3
UK COVID-Nation-New	healthcare	D	28	20	729	4	3
UK COVID-Nation-New	healthcare	W	8	4	105	4	3
UK COVID-UTLA-Cumulative	healthcare	W	13	5	104	214	1
UK COVID-UTLA-New	healthcare	D	28	10	721	214	1

C Sampling Details

C.1 Flexible Context Length and Horizon Sampling

Unlike decoder-only transformers that inherently support variable context and prediction lengths during pre-training, encoder-only architectures face significant challenges in achieving such flexible length settings, which is quite crucial for model generalization. Theoretically, while models pre-trained with fixed target horizon can perform arbitrary-length inference via auto-regression, they are susceptible to the cumulative error propagation common in decoder-only structures. To address this, we implement flexible context length and horizon during the sampling stage. Specifically, for each sampled entity e_i with context length L_i and target horizon T_i , we construct each batch by left-padding input contexts with NaN values to the batch-wise maximum input length $L_{\max} = \max\{L_i\}_{i=1}^N$. Meanwhile, target outputs are right-padded to a pre-defined maximum horizon $T_{\max} = 480$, corresponding to 30 output tokens with patch length $L_p = 16$. The padded context positions, together with invalid observations, constitute the binary observation mask \mathcal{M} , while the padded target segments are excluded from the final loss calculation. Such flexible sampling strategy effectively enhances the predictive generalization of **Falcon-X**.

C.2 Runtime Multivariate Sampling

To mitigate potential GPU memory bottlenecks arising from multivariate sampling, we adopt a dynamic variate sampling strategy at runtime. After flexible context length and horizon sampling, for each entity e_i with v_i variates, we first randomly permute the variate order to reduce order bias and encourage permutation-robust, content-driven cross-variate modeling, consistent with prior findings that channel shuffling improves robustness to channel ordering in multivariate forecasting (Xu et al., 2026). Then we traverse variates in the permuted order. Subsequently, we iteratively append valid variates to the training sample until all candidates are processed or a pre-defined per-sample limit, M_{\max} , is reached. Finally, entity e_i contributes $m_i = \min(v_i, M_{\max})$ variates. This runtime design naturally supports heterogeneous variate dimensionalities and prevents dimensionality-related computational bottlenecks while facing excessively large v_i .

After variate selection, multivariate samples may still vary in variate count. To batch them efficiently, we enforce a batch-level variate budget and accumulate samples until the total number of retained variates reaches a preset threshold, stabilizing memory usage across training steps. This variate-wise batching strategy substantially reduces channel-padding waste and enables efficient training on multivariate data with highly variate dimensionality.

D Additional Visualization

We provide visualizations of **Falcon-X**'s quantile forecasts across representative datasets at different frequencies $\{5T, 15T, 10S, H\}$ and prediction horizons $T = \{48, 60, 480, 720\}$. Specifically, Figure 10 shows medium-horizon ($T = 480$) forecasts for Loop Seattle/H, Figure 11 for KDD Cup 2018/H, and Figure 12 for Electricity/H at $T = 720$. Figure 13 presents forecasts on Bitbrains Fast Storage/5T at $T = 48$, where the two channels exhibit strong positive correlation, which **Falcon-X** accurately captures. In contrast, Figure 14 shows forecasts on Bizitobs Application/10s at $T = 60$, where two channels are negatively correlated, and **Falcon-X** successfully models the inverse relationship. These results demonstrate that the variable-to-prototype design effectively captures both positive and negative inter-variable dependencies, and preserves temporal consistency across diverse datasets. Moreover, the visualizations highlight **Falcon-X**'s robustness in handling different sampling frequencies and prediction horizons without manual adjustment.

Moreover, we visualize **Falcon-X**'s medium-horizon ($T = 480$) quantile forecasts on ETTh1/15T and ETTh1/H, comparing results with and without multivariate inference across all seven channels. As shown in Figure 15 and Figure 16, enabling multivariate inference allows **Falcon-X** to more accurately capture complex inter-variable relationships, including both strong and subtle dependencies, which results in tighter predictive intervals and improved alignment with observed dynamics across channels.

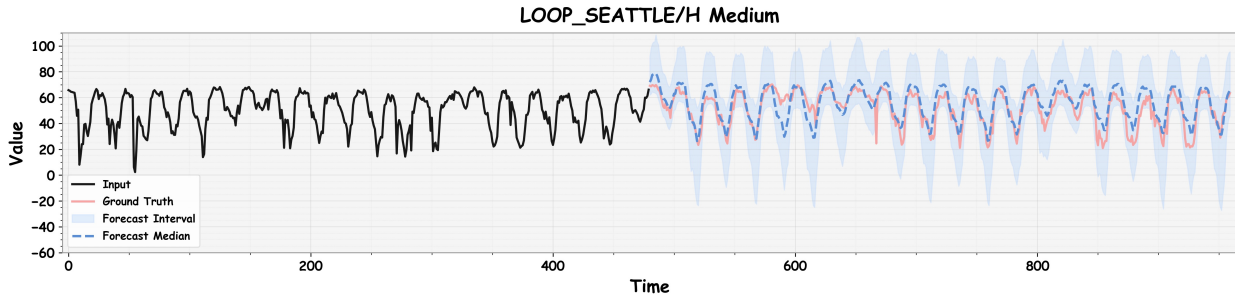


Figure 10 Medium-horizon ($T = 480$) quantile forecasts on Loop Seattle.

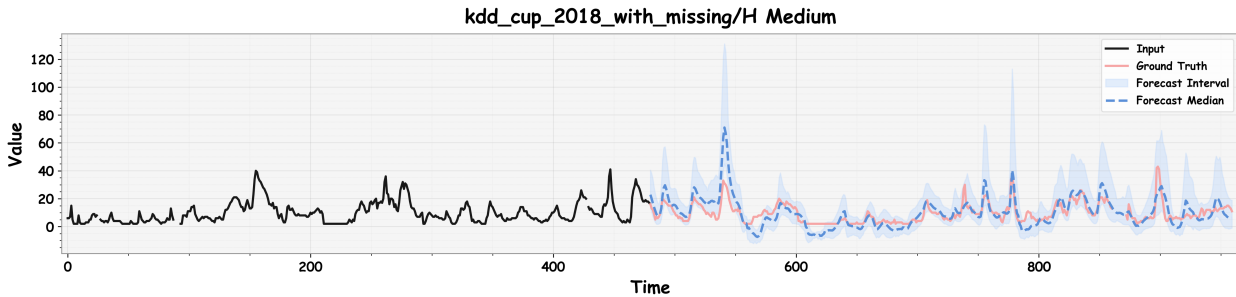


Figure 11 Medium-horizon ($T = 480$) quantile forecasts on kdd cup 2018.

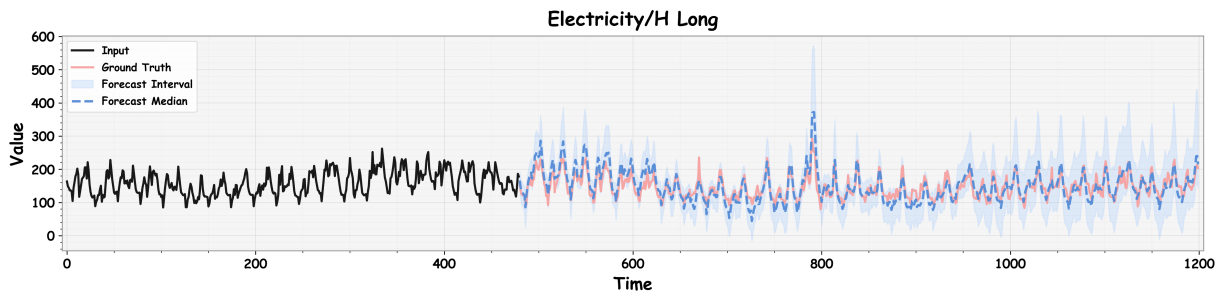


Figure 12 Long-horizon ($T = 720$) quantile forecasts on Electricity.

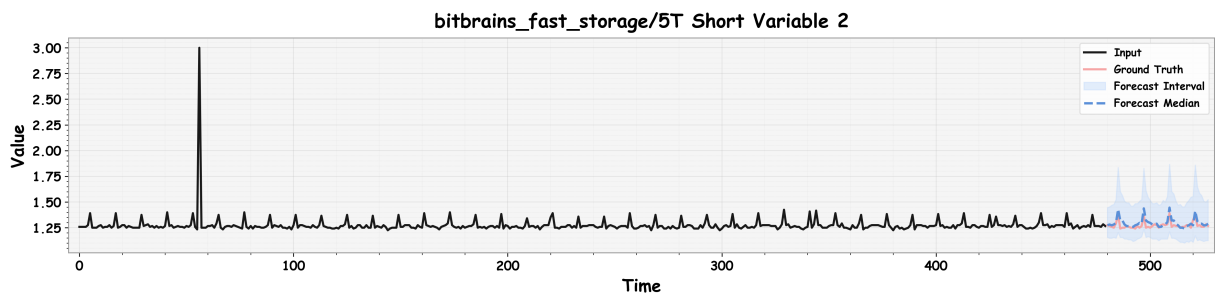
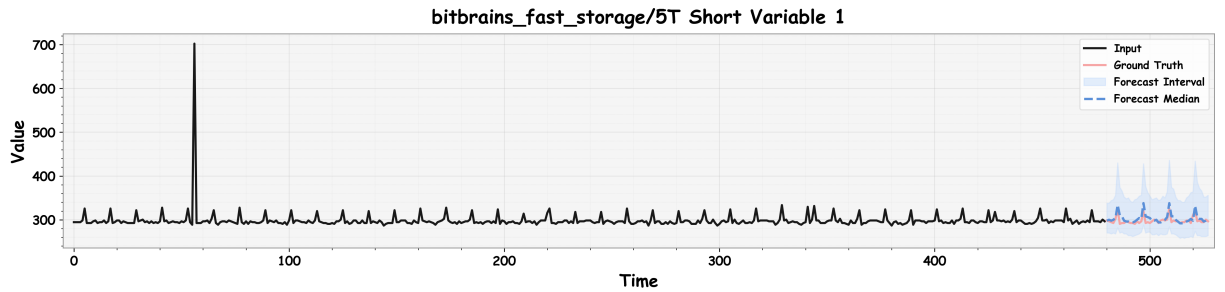


Figure 13 Short-horizon ($T = 48$) quantile forecasts on bitbrains fast storage.

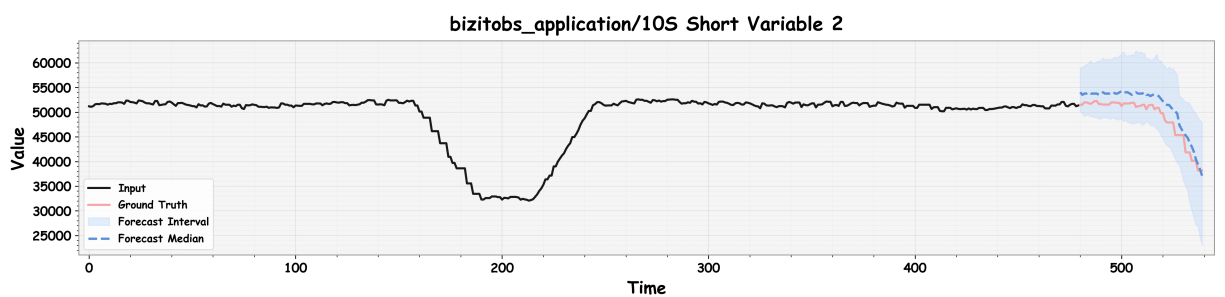
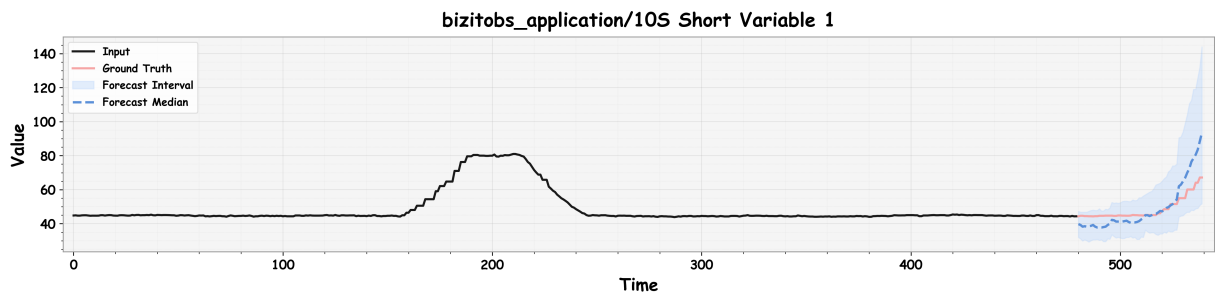


Figure 14 Short-horizon ($T = 60$) quantile forecasts on bizitobs application.

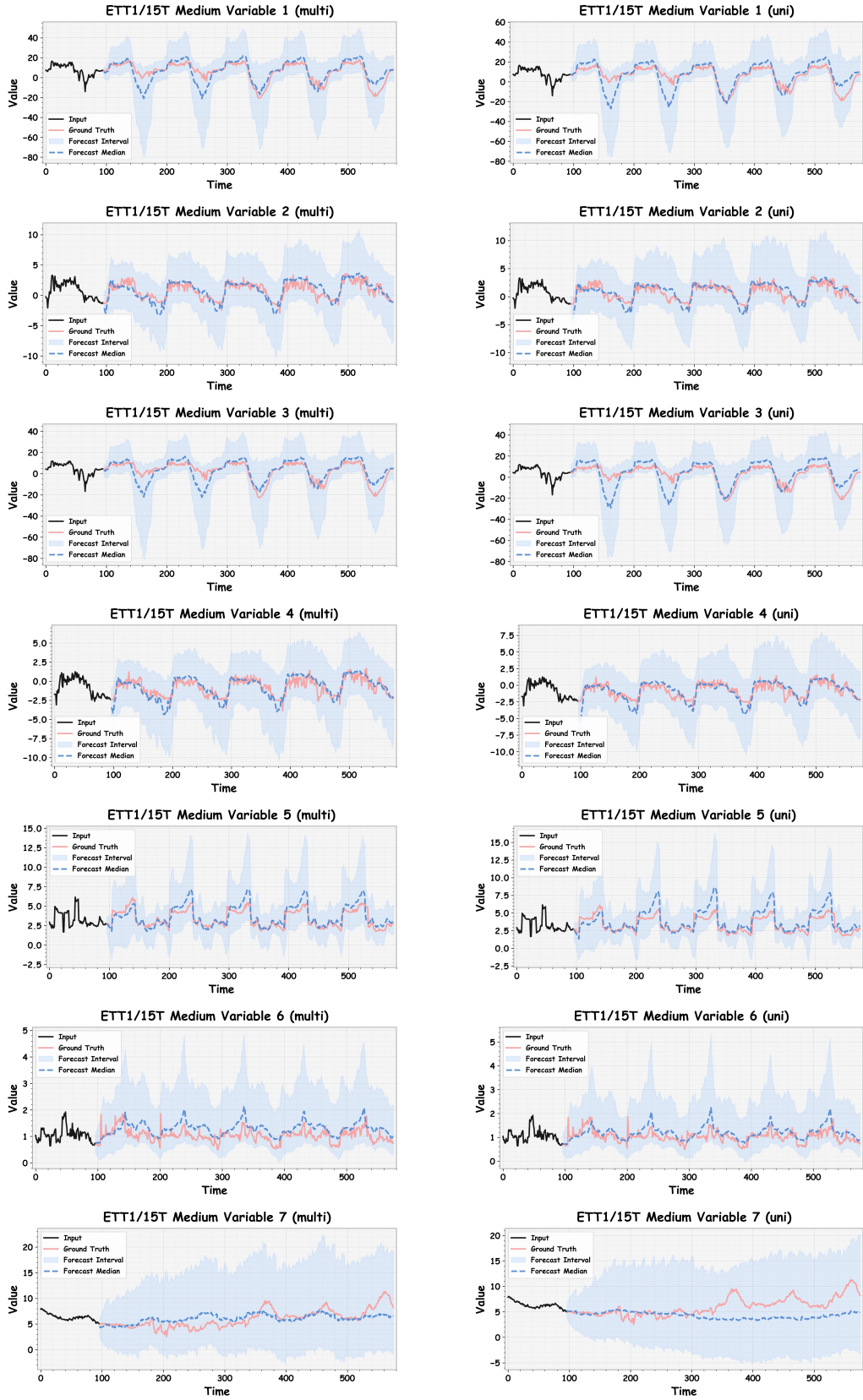


Figure 15 Medium-horizon ($T = 480$) quantile forecasts on ETT1/15T with 7 channels, comparing Falcon-X with and without multivariate inference.

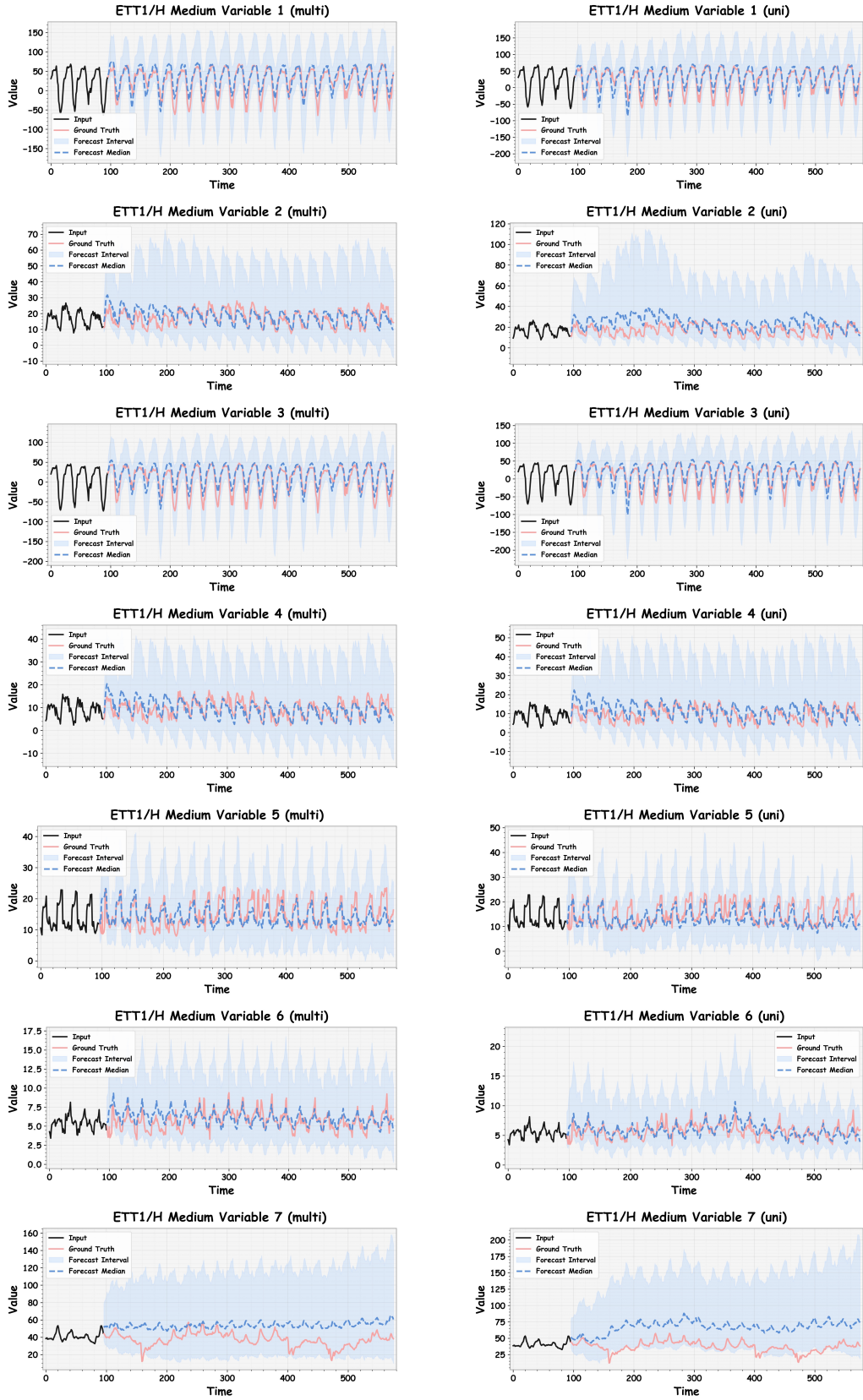


Figure 16 Medium-horizon ($T = 480$) quantile forecasts on ETT1/H with 7 channels, comparing **Falcon-X** with and without multivariate inference.